

Position: Evaluation of ECG Representations Must Be Fixed

Zachary Berger^{1,2*} Daniel Prakah-Asante^{1,2*} John Guttag¹ Collin M. Stultz^{1,2}

Abstract

This position paper argues that current benchmarking practice in 12-lead ECG representation learning must be fixed to ensure progress is reliable and aligned with clinically meaningful objectives. The field has largely converged on three public multi-label benchmarks (PTB-XL, CPSC2018, CSN) dominated by arrhythmia and waveform-morphology labels, even though the ECG is known to encode substantially broader clinical information. We argue that downstream evaluation should expand to include an assessment of structural heart disease and patient-level forecasting, in addition to other evolving ECG-related endpoints, as relevant clinical targets. Next, we outline evaluation best practices for multi-label, imbalanced settings, and show that when they are applied, the literature’s current conclusion about which representations perform best is altered. Furthermore, we demonstrate the surprising result that a randomly initialized encoder with linear evaluation matches state-of-the-art pre-training on many tasks. This motivates the use of a random encoder as a reasonable baseline model. We substantiate our observations with an empirical evaluation of three representative ECG pre-training approaches across six evaluation settings: the three standard benchmarks, a structural disease dataset, hemodynamic inference, and patient forecasting.

1. Introduction

Representation learning aims to produce features that are useful across many downstream applications. This reduces reliance on large labeled datasets to learn task-specific models (Bengio et al., 2013). However, there is a tension between learning features that are broadly useful versus those that excel for particular tasks (Bommasani et al., 2022). This

*Equal contribution ¹Massachusetts Institute of Technology, Cambridge, MA, USA ²Massachusetts General Hospital, Boston, MA, USA. Correspondence to: Zachary Berger <zberger@mit.edu>.

Preprint. February 20, 2026.

tension is pronounced in medicine, where labeled data can be sparse and clinical use-cases varied (Esteva et al., 2019).

In medicine, what constitutes a meaningful endpoint task depends on the modality. For example, the clinical targets of chest X-ray differ from those of electroencephalography. As a result, benchmarking practice in medicine must be discussed on a per-modality basis. These choices shape which representations appear effective and steer subsequent methodological development (Lipton & Steinhardt, 2019; Pineau et al., 2021).

Here, we focus on the 12-lead electrocardiogram (ECG), an inexpensive and commonly used diagnostic tool that non-invasively records the heart’s electrical activity (Noble et al., 1990). ECG representation learning is an active area of research and has recently received attention in major ML venues (e.g., ICML, ICLR, NeurIPS, AAAI) (Liu et al., 2024b; Hung et al., 2024; Wang et al., 2025; Na et al., 2024; Jin et al., 2025; Chen et al., 2025; Lan et al., 2022). As the literature grows, we argue it is timely to re-examine the field’s current benchmarking practice. A rigorous and uniform benchmarking strategy is essential to ensure reliable and reproducible results, and most importantly that the learned representations align with clinically meaningful objectives. Lastly, ECG benchmarking is associated with a number of challenges, including the use of large multi-label and severely imbalanced datasets – a structure common across many applied machine learning (ML) settings (Zhang & Zhou, 2014; He & Garcia, 2009).

In this position paper, we analyze how current task selection and reporting practice shape conclusions about ECG representation quality. We then evaluate these choices empirically across three representative pre-training methods and six evaluation settings.

Three datasets have become standard for evaluating 12-lead ECG representations: PTB-XL (Wagner et al., 2020), CPSC2018 (Liu et al., 2018), and CSN (Zheng et al., 2020). Each is a multi-label suite focused primarily on binary arrhythmia outcomes and waveform morphology classification. However, the ECG has increasingly been recognized to contain information pertinent to a wider variety of relevant outcomes, e.g., structural disease (Poterucha et al., 2025), hemodynamic state (Schlesinger et al., 2022), and patient forecasting (Khurshid et al., 2022; Bergamaschi et al., 2025).

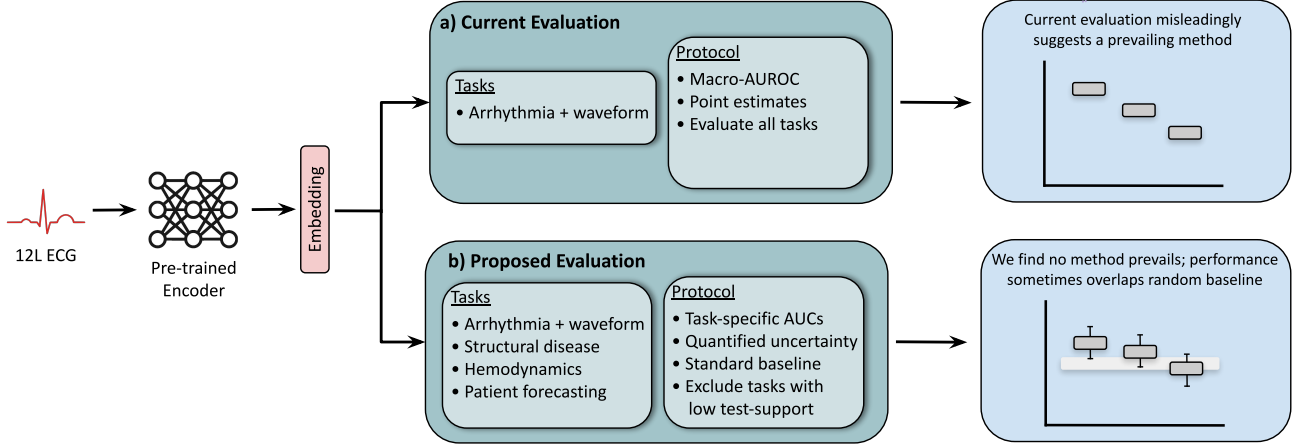


Figure 1. Overview of the evaluation pipeline for 12-lead ECG representations. (a) Current practice focuses on arrhythmia/waveform tasks and macro-AUROC point estimates, which can produce misleading method rankings. (b) We propose a broader set of clinically relevant tasks and evaluation best-practices that more reliably assess methods. We find that no method consistently prevails and for many tasks, many methods overlap with the baseline of a randomly initialized encoder.

In Section 3, we propose additional tasks that would be a welcome addition in the evaluation pipeline. This is particularly relevant as the field moves towards more complex tasks, where ECGs are combined with other modalities to predict clinical outcomes that are not deterministic functions of the ECG alone.

To manage multi-label evaluation across many tasks, the field has largely converged on summarizing performance with macro-AUROC, which aggregates per-label AUROCs through an unweighted mean (Zhang & Zhou, 2014). This convention enables straightforward comparison across methods, but obscures clinically meaningful behavior. Clinicians ultimately deploy models for specific purposes, yet macro-AUROC masks performance on individual endpoints by collapsing them into a single number. This issue is compounded by severe label imbalance; many ECG labels have few positive examples, yielding noisy task-level estimates. However, uncertainty is seldom reported alongside headline metrics. Moreover, AUROC alone can misrepresent performance on imbalanced labels, where alternative metrics may better reflect clinical utility (Davis & Goadrich, 2006; Saito & Rehmsmeier, 2015). In Section 4, we suggest a set of reporting and evaluation best-practices and show that many prior studies do not adhere to them.

In Section 5, we show that applying these practices can change method rankings on standard benchmarks and alter conclusions of the current literature about which methods perform best. We also show that a randomly initialized encoder with linear evaluation matches the performance of state-of-the-art ECG pre-training methods on many individual tasks.

Our position is visualized in Figure 1. We argue that going forward, evaluation of representations of ECG should

- Cover a wider variety of tasks than is currently typical. For example, they should include prediction of patient outcomes or estimates of structural disease rather than just arrhythmia and waveform classification.
- Report clinically relevant task-specific findings rather than focus, as most papers do, on aggregate performance. For example, they should report on AUROC, precision, and recall for individual tasks rather than just macro-AUROC over classes of tasks.
- Carefully characterize uncertainty, which can be quite high for tasks with a small number of positive examples, which is common in ECG datasets.
- Compare the utility of learned representations to that of a simple baseline: a randomly initialized encoder.

2. Related Work

Benchmarking in ML. Progress in empirical ML has long been driven by benchmarks (e.g., Geiger et al., 2012; Lin et al., 2014; Russakovsky et al., 2015; Wang et al., 2018). However, evaluation practices often lack rigor and standardization across studies (Lipton & Steinhardt, 2019; Liao et al., 2021; Herrmann et al., 2024). This has motivated a growing body of work that critically examines and improves benchmark design and reporting (e.g., Gebru et al., 2021; Pineau et al., 2021; Vendrow et al., 2025). Many important lessons have emerged from analyses of domain-specific settings, for instance, in recommendation systems (Ferrari Dacrema et al., 2019), neural network pruning (Blalock et al., 2020), anomaly detection (Liu & Paparrizos, 2024), and graph learning (Bechler-Speicher et al., 2025).

ECG Benchmarking. ECGs are routinely collected in

clinical care, so large labeled corpora exist in many health systems. Yet, these data are rarely shared because of patient privacy constraints and institutional requirements. As a result, despite the volume of ECGs that exist, there are few open-source datasets.

In response, the community has largely repurposed the available public datasets for downstream benchmarking of ECG representations. Evaluations typically center around three datasets, CPSC2018 (Liu et al., 2018), PTB-XL (Wagner et al., 2020; 2022), and CSN (Zheng et al., 2020; 2022), which contain on the order of tens of thousands of recordings. All three focus narrowly on arrhythmia and waveform abnormality labels. Several other datasets with similar labels are occasionally used for testing, or aggregated together for training (e.g., Perez Alday et al., 2022; Liu et al., 2022; Ribeiro et al., 2020).

MIMIC-IV (Gow et al., 2023; Goldberger et al., 2000) and CODE-15 (Ribeiro et al., 2020) are commonly used for pre-training, since they are large open-source datasets. MIMIC-IV is of particular importance because its ECGs are linked to electronic health record data. This enables learning algorithms that incorporate clinical context through multi-modal supervision, and has garnered state-of-the-art performance (Liu et al., 2024b; Hung et al., 2024). Many studies pre-train on private institutional data (e.g., Diamant et al., 2022) or semi-restricted resources (e.g., Sudlow et al., 2015; Littlejohns et al., 2020; Koscova et al., 2024). While these datasets can be valuable for scaling up training data, their restricted access limits reproducibility.

There are few open-access datasets that expand beyond arrhythmia and waveform abnormality labels. A notable recent release is EchoNext, which links ECGs to echocardiography-derived ground truth to study structural heart disease (Poterucha et al., 2025).

Several pre-prints contemporaneous to this work have taken initial steps toward improving benchmarking for ECG representation learning (Lunelli et al., 2025; Al-Masud et al., 2025; Wan et al., 2025). These efforts each aim to consolidate evaluation practices in an open-source framework. However, they do not implement all of the protocol recommendations we discuss in Section 4. They also do not yet capture the breadth of clinically grounded tasks we argue the field should work toward in Section 3.

ECG Representation Learning. Self-supervised pre-training is a standard paradigm, driven by successes in computer vision (Chen et al., 2020) and natural language processing (Devlin et al., 2019). Early ECG representation learning (Kiyasseh et al., 2021; Mehari & Strothoff, 2022) adapted popular vision frameworks such as SimCLR (Chen et al., 2020) and BYOL (Grill et al., 2020). These are now widely used as baselines in the ECG literature.

Many specialized methods have introduced inductive biases specific to 12-lead ECGs. These often take inspiration from contrastive learning and reconstruction-based learning.

Contrastive methods learn representations by bringing together related samples while maximizing the distance between unrelated samples. These positive and negative pairs can be generated through augmentation (Chen et al., 2020; Grill et al., 2020; Chen & He, 2020; Chen et al., 2021) or by relying on clinical structure, for example, patient identity (Diamant et al., 2022). CLOCS (Kiyasseh et al., 2021) is a popular ECG-specific approach that builds pairs directly from the temporal and lead-structure of the signal.

Reconstruction-based methods optimize representations by compressing then reconstructing examples directly, often by masking then filling in part of the signal (He et al., 2021; Na et al., 2024; Zhang et al., 2023a;b).

In parallel, recent work uses multi-modal supervision, commonly pairing ECGs with clinical text from the electronic health record (Lalam et al., 2023; Yu et al., 2024). MERL (Liu et al., 2024b) and D-BETA (Hung et al., 2024) have claimed state-of-the-art performance following this approach. MERL aligns ECG embeddings with representations of their paired text reports using a contrastive objective. D-BETA extends this work by regularizing the learning process with reconstruction loss on the text and ECG.

In this paper, we characterize the state of benchmarking for ECG representation learning by surveying work published at major ML conferences since 2019. We also include approaches cited by those publications. When making broad claims about the field, we refer to this *survey set* of 28 methods; details are provided in Appendix A. We note that many more pre-trained ECG models have been proposed, some of which are covered in the review of (Han et al., 2025).

For our empirical study, we focus on CLOCS, MERL, and D-BETA as exemplar methods. CLOCS and MERL are widely cited, and D-BETA is a recent purported state-of-the-art approach. All three are supported by released weights or pre-training code.

3. Extending beyond current benchmarks to more holistic clinical applications

Since its invention, the ECG has primarily been used to diagnose arrhythmias and waveform abnormalities (Rivera-Ruiz et al., 2008; Fisch, 2000). As a result, downstream evaluation of ECG representations has been based largely on how they perform on such tasks. In our survey of 28 ECG representation learning papers, 23 report results on PTB-XL, 15 on CPSC2018, 11 on CSN or its constituent datasets Chapman-Shaoxing and Ningbo, with 25 evaluating on at least one of the three (see Table 7).

Table 1. According to macro-AUROC, MERL and D-BETA appear to consistently dominate. However, once uncertainty is quantified, no ECG pre-training method consistently prevails. A randomly initialized encoder is often competitive, sometimes beating the ECG-specific pre-training method CLOCS. Entries report macro-AUROC with 95% confidence intervals in the subscript under linear probing at varying levels of training data. Green highlight indicates that method is the best performing within sampling noise.

Dataset		Random	CLOCS	MERL	D-BETA
PTB-XL	1%	0.596 0.583–0.609	0.756 0.744–0.767	0.809 0.799–0.819	0.856 0.847–0.865
	10%	0.831 0.821–0.841	0.809 0.798–0.819	0.879 0.871–0.887	0.885 0.877–0.894
	100%	0.861 0.852–0.869	0.821 0.811–0.831	0.903 0.896–0.910	0.893 0.885–0.901
SUB	1%	0.603 0.588–0.616	0.679 0.664–0.692	0.729 0.717–0.741	0.758 0.746–0.769
	10%	0.734 0.712–0.757	0.740 0.713–0.770	0.836 0.820–0.852	0.857 0.843–0.871
	100%	0.838 0.813–0.863	0.782 0.754–0.811	0.903 0.887–0.916	0.893 0.880–0.906
PTB-XL	1%	0.553 0.535–0.570	0.585 0.569–0.600	0.619 0.602–0.635	0.674 0.652–0.693
	10%	0.587 0.567–0.607	0.636 0.613–0.660	0.741 0.715–0.768	0.780 0.751–0.807
	100%	0.678 0.656–0.699	0.717 0.690–0.741	0.835 0.820–0.851	0.829 0.806–0.853
RHYTHM	1%	0.563 0.551–0.574	0.617 0.606–0.627	0.668 0.660–0.676	0.721 0.715–0.726
	10%	0.668 0.609–0.723	0.775 0.735–0.810	0.877 0.855–0.897	0.943 0.923–0.961
	100%	0.746 0.698–0.791	0.825 0.790–0.857	0.886 0.839–0.933	0.969 0.957–0.978
CPSC2018	1%	0.604 0.590–0.617	0.683 0.669–0.696	0.720 0.707–0.733	0.874 0.866–0.882
	10%	0.794 0.778–0.808	0.763 0.747–0.778	0.898 0.889–0.908	0.942 0.932–0.951
	100%	0.849 0.836–0.861	0.809 0.796–0.821	0.931 0.923–0.939	0.957 0.947–0.965
CSN	1%	0.559 0.549–0.568	0.629 0.618–0.639	0.660 0.649–0.671	0.734 0.729–0.738
	10%	0.654 0.641–0.667	0.716 0.701–0.731	0.789 0.776–0.801	0.836 0.829–0.843
	100%	0.780 0.757–0.802	0.805 0.789–0.820	0.910 0.897–0.924	0.949 0.941–0.956
ECHONEXT	1%	0.685 0.671–0.700	0.621 0.607–0.634	0.673 0.658–0.687	0.690 0.675–0.705
	10%	0.744 0.732–0.757	0.679 0.667–0.691	0.745 0.729–0.760	0.740 0.728–0.751
	100%	0.770 0.756–0.783	0.713 0.702–0.724	0.795 0.785–0.805	0.765 0.754–0.775

Recently, there has been interest in using the ECG for clinical tasks other than arrhythmia and waveform abnormality classification. It has been shown that machine-learned models can be applied to the ECG to infer clinically-relevant endpoints that are not readily visible in the signal (Friedman et al., 2025). Downstream evaluation of ECG representations should expand to better reflect this clinical scope.

We propose the following families of downstream tasks. Our categorization is motivated by the physiological view of the heart as an electromechanical pump that generates pressure gradients and blood flow (Nerbonne & Kass, 2005; Fukuta & Little, 2008).

1. **Arrhythmia and Waveform Abnormalities** include tasks derived from expert interpretation of the ECG trace. Many public datasets, e.g., PTB-XL, CPSC2018, and CSN (Wagner et al., 2020; Liu et al., 2018; Zheng et al., 2020) include relevant labels.

2. **Structural Disease** involves tasks that probe the heart’s morphology, such as systolic function and valvular disease. Labels for these are often derived from contemporaneous imaging including echocardiography and cardiac MRI. EchoNext is an open-source dataset of paired ECG and echocardiogram findings containing relevant labels (Poterucha et al., 2025).
3. **Hemodynamic State** targets inference of cardiac filling pressures, e.g., mean pulmonary capillary wedge pressure (mPCWP) and flows (Schlesinger et al., 2022). Ground truth for these labels often comes from right heart catheterization. Much of the literature on these tasks use proprietary data. Publicly, MIMIC-IV contains some paired bedside-monitor ECG and invasive blood pressure signals (Moody et al., 2022).

In addition to task family, downstream targets can be separated into *diagnosis* and *patient forecasting*. *Diagnosis*

involves estimating patient state at the time of an ECG, e.g., if a patient currently exhibits a left ventricular ejection fraction (LVEF) below 40%. *Patient forecasting* involves risk prediction over a future horizon, e.g., will a patient develop LVEF below 40% within 1-year.

In Section 5, we evaluate current ECG representations on exemplar tasks from the taxonomy defined above. We find that performance can vary widely across the different kinds of tasks. Additionally, we note that our proposed taxonomy is a starting point rather than an exhaustive catalog of ECG applications. We believe the community must come to a consensus on a set of clinically grounded tasks.

4. Toward evaluation best-practices that reliably stratify representation quality

An evaluation protocol should *reliably stratify* representation quality, so that method rankings are robust to reasonable resampling and reporting choices. Unfortunately, much of the literature presents results in a way that obscures whether one representation is meaningfully better than another.

First, the field relies on macro-AUROC (Wu & Zhou, 2017) as its primary metric. In our survey, 89.29% of papers reported it as their headline metric. While convenient for evaluating multi-label data, macro-AUROC masks performance on the individual clinical tasks that clinicians care about. Furthermore, macro-averaging weights all labels equally. This implicitly grants rare, high-variance endpoints the same influence as common and clinically salient ones, amplifying noise in reported rankings. However, 35.71% of papers did not report per-task performance.

Second, ECG benchmarks often include rare diagnoses that yield highly imbalanced labels with few positive examples. For example, under the standard PTB-XL protocol, 13 labels have fewer than 10 examples in the test set, yet the protocol explicitly retains these labels for evaluation (Wagner et al., 2020; Strothoff et al., 2021). In this case, per-label performance metrics have high sampling variability and can shift meaningfully because of small perturbations during resampling. Macro-AUROC inherits this variability, and can amplify it by giving equal-weight to all labels.

Under extreme class imbalance, AUROC can remain deceptively high even when a model yields low precision at clinically relevant operating points. In this case, AUPRC is a more appropriate metric (Davis & Goadrich, 2006; Saito & Rehmsmeier, 2015).

Lastly, uncertainty is rarely quantified in the field; 42.86% papers did not report confidence intervals for their main results. As a result, many apparent gaps between methods are indistinguishable from sampling noise.

We advocate for a standardized and statistically rigorous

reporting protocol. The following practices are broadly applicable to multi-label benchmarks:

1. Treat macro-averaged metrics as a coarse summary of model performance; report per-task AUROC and AUPRC.
2. Report bootstrapped confidence intervals, not only point estimates.
3. Use paired comparisons for claims of improvement over prior methods, for example, with paired bootstrap confidence intervals or statistical tests.
4. Exclude labels with insufficient number of test-set examples from quantitative evaluation.

ECG datasets have dozens of labels, so exhaustive reporting may be impractical in the main text of a work. However, these data should be available in the supplementary material. We recommend emphasizing the most clinically salient endpoints, for example, diagnosis of low ejection fraction. These core labels should be agreed upon by the community to enable meaningful comparison and mitigate cherry-picking results.

The importance of these recommendations is made transparent in Section 5 where we demonstrate that following them changes what one might conclude about the relative performance of current methods.

5. Empirical Study

5.1. Pre-training Configuration

Models. We evaluate downstream performance using representations from three pre-trained ECG encoders: CLOCS (Kiyasseh et al., 2021), MERL (Liu et al., 2024b), and D-BETA (Hung et al., 2024). As a baseline, we also evaluate embeddings from a randomly initialized 1D ResNet-18 encoder, a common architecture in ECG modeling (He et al., 2016; Ribeiro et al., 2020).

Pre-training Dataset. We use the MIMIC-IV ECG database (Gow et al., 2023), which contains 800,035 10-second 12-lead ECGs collected from 161,352 patients. Each ECG is paired with a text diagnosis report.

Implementation. We use publicly available MIMIC-IV checkpoints for MERL and D-BETA, published by their respective authors. For CLOCS, we retrain on MIMIC-IV following the authors’ training procedures so that all models are pre-trained on the same corpus; this isolates differences caused by model design and objective rather than pre-training data. Full pre-training details are provided in Appendix C.2. All experiments are conducted on one NVIDIA Tesla V100-SXM2-32GB GPU.

Table 2. Task-level results reveal heterogeneous behavior. Shown are the five highest-prevalence PTB-XL SUB labels plus CLBBB. Method rankings vary by endpoint. AUPRC can help capture differences masked by AUROC, as in the case of CLBBB. Each cell reports AUROC (top) and AUPRC (bottom) with 95% confidence intervals; methods statistically indistinguishable from the best (overlapping intervals) are highlighted in green. Performance on the remaining tasks are in Table 10.

Method	NORM	IMI	AMI	STTC	LVH	CLBBB
Random	0.888 0.874–0.901 / 0.835 0.811–0.860	0.857 0.835–0.877 / 0.521 0.470–0.572	0.891 0.871–0.910 / 0.605 0.553–0.661	0.820 0.794–0.845 / 0.307 0.263–0.355	0.924 0.907–0.941 / 0.631 0.569–0.694	0.994 0.989–0.998 / 0.855 0.748–0.940
CLOCS	0.858 0.843–0.873 / 0.786 0.760–0.812	0.675 0.644–0.706 / 0.304 0.263–0.352	0.855 0.830–0.879 / 0.576 0.522–0.628	0.820 0.792–0.845 / 0.311 0.269–0.357	0.910 0.889–0.929 / 0.588 0.525–0.649	0.982 0.968–0.990 / 0.642 0.522–0.764
MERL	0.922 0.910–0.933 / 0.876 0.853–0.898	0.837 0.813–0.859 / 0.517 0.464–0.569	0.957 0.946–0.967 / 0.833 0.799–0.865	0.881 0.862–0.900 / 0.451 0.392–0.514	0.930 0.912–0.945 / 0.665 0.604–0.720	0.999 0.997–1.000 / 0.938 0.877–0.984
D-BETA	0.929 0.918–0.939 / 0.894 0.875–0.912	0.897 0.880–0.914 / 0.691 0.646–0.734	0.954 0.941–0.966 / 0.824 0.782–0.863	0.859 0.834–0.883 / 0.423 0.369–0.488	0.859 0.835–0.882 / 0.455 0.389–0.523	0.999 0.997–1.000 / 0.969 0.932–0.996

5.2. Downstream Tasks

We evaluate all ECG encoders with linear probing on six downstream settings. Full dataset details, including label definitions and prevalence, are provided in Appendix B.

All ECGs are standardized to a 10-second 12-lead segment in millivolts sampled at 500 Hz. We remove recordings that have a NaN or Inf sample. We split data into train/val/test partitions (70/10/20), except for PTB-XL and EchoNext, which use standard splits, and the patient forecasting task, whose authors follow a 75/10/15 split (Poterucha et al., 2025; Strothoff et al., 2021; Bergamaschi et al., 2025).

PTB-XL. PTB-XL consists of 21,837 12-lead 10-second ECGs from 18,885 patients (Wagner et al., 2022). It is split into four multi-label classification tasks that assess arrhythmia and waveform abnormalities, with varying numbers of binary targets: SUPER (5 labels), SUB (23 labels), FORM (19 labels), and RHYTHM (12 labels). Each task has a different number of samples, detailed in Appendix B.1.

CPSC2018. This dataset includes 6,877 12-lead ECGs, with arrhythmia and waveform morphology annotations (Liu et al., 2018). Recording duration varies between 5 and 72 seconds. We exclude recordings shorter than 10 seconds, and for longer recordings, clip them to 10 seconds. Appendix B.2 contains more details.

CSN. The Chapman-Shaoxing-Ningbo (CSN) database includes 45,152 10-second 12-lead ECGs from 10,646 patients (Zheng et al., 2022). ECGs are annotated with arrhythmia and waveform morphology labels; see Appendix B.3.

EchoNext. For binary classification of structural heart disease from the ECG, we use EchoNext, a dataset of 100,000 10-second 12-lead ECGs (Poterucha et al., 2025). Each ECG was paired with a contemporaneous echocardiogram, from which structural heart disease labels were derived. Details are in Appendix B.4.

Hemodynamic Inference. We use a private dataset of 9,226 10-second 12-lead ECGs from 5,072 patients at Massachusetts General Hospital (MGH) to evaluate hemodynamic inference (Schlesinger et al., 2022). We consider two diagnosis tasks, inferring contemporaneous mean pulmonary capillary wedge pressure (mPCWP) and mean pulmonary artery pressure (mPA) as measured by ground-truth right heart catheterization. Cohort construction and labeling are described in Appendix B.5.

Patient Forecasting. We consider the binary prediction task of whether a patient will experience heart failure within one year of an ECG (1YR-HF). We define heart failure as echocardiographic left ventricular ejection fraction below 40%. We use the private dataset of (Bergamaschi et al., 2025), which includes 913,420 10-second 12-lead ECGs from 82,244 patients at MGH. See Section B.6.

5.3. Evaluation Protocol

We evaluate the downstream performance of each representation using linear probing. For each individual task, we freeze the ECG encoder and train a single linear layer on top of the embeddings using the labeled training set. We run a hyperparameter sweep, detailed in Appendix C.1, and pick the best probe for each task based on the validation set. We then evaluate that probe on the test set.

We report the AUROC and AUPRC for each individual task. We additionally aggregate over tasks to report the macro-AUROC for each dataset. To quantify uncertainty, for all experiments, we conduct a paired bootstrap with 1,000 resamples with replacement on the test set and report 95% confidence intervals.

To assess performance in a limited-label regime, on PTB-XL, CPSC2018, CSN, and EchoNext, we repeat this probing procedure using 1%, 10%, and 100% of the available labeled training data.

5.4. Experimental Results

5.4.1. EVALUATION ON PTB-XL, CPSC2018, CSN

Macro Performance. Table 1 shows that conclusions drawn from macro-AUROC can change substantially once a random encoder baseline and uncertainty are included. MERL and D-BETA generally outperform a randomly initialized encoder in the extremely low-label regime (1%), with D-BETA achieving the strongest macro-AUROC. However, as label availability increases, the random encoder improves sharply and often matches or exceeds CLOCS, an ECG-specific contrastive method, including on PTB-XL SUPER/SUB and CPSC2018 at 100% data. Moreover, no single pre-training method dominates across evaluation settings: MERL matches or surpasses D-BETA on PTB-XL SUB/FORM, where CLOCS under-performs even relative to random. Finally, many differences between MERL and D-BETA fall within overlapping 95% confidence intervals, indicating that rankings based solely on macro-AUROC point estimates can be unreliable.

Task-level Performance. We next examine task-level performance within each dataset. Full results are available in Appendices D.1, E, and F. We report results for the five labels with highest prevalence from PTB-XL SUB in Table 2. We also include complete left bundle branch block (CLBBB) as an interesting case where all models perform near-perfectly according to AUROC, motivating the need for AUPRC to distinguish representation quality.

The task-level view is more nuanced than the macro measures. In Table 2, the randomly initialized encoder is consistently competitive with CLOCS, and is the best-performing within sampling noise on LVH and CLBBB. While MERL and D-BETA provide modest gains on some tasks (e.g., AMI), the relative ranking between MERL and D-BETA depends on the endpoint. Finally, CLBBB illustrates why AUROC alone can be misleading: AUROC is near-saturated for all methods, whereas AUPRC reveals better separation, with MERL and D-BETA substantially outperforming CLOCS and typically exceeding the random baseline.

5.4.2. SENSITIVITY OF MACRO-AVERAGED METRICS TO LABELS WITH FEW EXAMPLES

In Section 4, we claim that the current practice of retaining labels with low test-support leads to noisy performance metrics. To illustrate this point, Table 3 highlights the AUROC for the three tasks with the lowest prevalence in PTB-XL FORM. Each task has small test-support (PRC(S): 1 positive, STE₊: 3 positives, TAB₋: 3 positives), producing very wide confidence intervals and highly variable AUROC estimates across resamples. This variance has a material effect on the resulting macro-AUROC for each model. To demonstrate this, when we remove the PTB-XL FORM labels with

Table 3. Tasks with very few positives yield high-variance estimates that can distort benchmark summaries. For the three tasks with lowest prevalence in PTB-XL FORM, confidence intervals are extremely wide, indicating that apparent differences are largely sampling noise. Each cell reports AUROC (top) and AUPRC (bottom) with 95% confidence intervals.

Method	PRC(S)	STE ₊	TAB ₋
Random	0.84 0.81–0.87 / 0.01 0.01–0.01	0.56 0.34–0.71 / 0.01 0.00–0.01	0.60 0.38–0.85 / 0.01 0.00–0.02
CLOCS	0.73 0.70–0.75 / 0.00 0.00–0.00	0.57 0.13–0.88 / 0.01 0.00–0.03	0.70 0.64–0.76 / 0.01 0.01–0.01
MERL	0.83 0.80–0.86 / 0.01 0.01–0.01	0.93 0.84–0.99 / 0.09 0.02–0.27	0.87 0.79–0.97 / 0.04 0.01–0.11
D-BETA	0.99 0.98–1.00 / 0.13 0.07–0.25	0.52 0.26–0.93 / 0.01 0.00–0.05	0.66 0.49–0.91 / 0.01 0.01–0.04

Table 4. Removing low-support labels can materially change macro-AUROC and alter which method appears most performant. ORIG uses the standard PTB-XL FORM test set; CLEAN excludes labels with fewer than 10 positive test examples. Values are macro-AUROC with 95% confidence intervals.

Method	ORIG	CLEAN	ΔMacro-AUROC
RANDOM	0.68 0.66–0.70	0.75 0.73–0.77	+0.076
CLOCS	0.72 0.69–0.74	0.72 0.69–0.74	-0.001
MERL	0.84 0.82–0.85	0.82 0.80–0.83	-0.020
D-BETA	0.83 0.81–0.85	0.85 0.83–0.86	+0.017

fewer than 10 positive test examples (4 labels in total), the resulting macro-AUROC shifts non-trivially. This is shown in Table 4, where there is a reversal of the apparent ordering between MERL and D-BETA (MERL decreases by 1.6 points while D-BETA increases by 1.7 points). Furthermore, Random experiences a +7.6 point boost on the restricted dataset. Parallel results for PTB-XL SUB and RHYTHM are provided in Appendix D.2.

5.4.3. EVALUATION ON ECHONEXT

We consider EchoNext to illustrate how conclusions about method quality differ on structural disease endpoints. Within EchoNext, CLOCS under-performs across all label budgets (Table 1). The Random baseline performs competitively to MERL and D-BETA at 1% and 10% of the data, falling within sampling noise. At 100% labels, MERL achieves the strongest macro-AUROC, modestly exceeding D-BETA, while Random remains a strong baseline. We further report performance on three clinically salient structural endpoints (Table 5); the same pattern holds at the task level, with CLOCS consistently worse and the other three methods tightly clustered.

5.4.4. HEMODYNAMIC INFERENCE

Table 6 shows results for the two hemodynamics tasks. Performance differences are smaller than on the standard pub-

Table 5. On structural disease endpoints, CLOCS under-performs while the other methods cluster closely. Each cell reports AUROC/AUPRC with 95% confidence intervals; best performing methods within sampling noise are highlighted in green.

Method	SHD	LVEF \leq 45	TR
Random	0.81 0.79–0.82 / 0.77 0.76–0.79	0.86 0.84–0.87 / 0.62 0.58–0.65	0.79 0.76–0.81 / 0.22 0.19–0.26
CLOCS	0.72 0.71–0.74 / 0.69 0.67–0.70	0.78 0.76–0.80 / 0.48 0.45–0.52	0.72 0.69–0.74 / 0.14 0.12–0.16
MERL	0.81 0.80–0.82 / 0.78 0.76–0.79	0.88 0.86–0.89 / 0.65 0.61–0.68	0.81 0.79–0.83 / 0.25 0.22–0.29
D-BETA	0.80 0.79–0.81 / 0.76 0.75–0.78	0.86 0.85–0.87 / 0.61 0.58–0.64	0.79 0.77–0.81 / 0.23 0.20–0.28

Table 6. Performance on mPCWP, mPA, and 1YR-HF (AUROC/AUPRC; 95% CIs). MERL and D-BETA prevail on 1YR-HF, but perform within sampling noise of the random baseline on the hemodynamic tasks.

Method	mPCWP	mPA	1YR-HF
Random	0.70 0.67–0.73 / 0.71 0.68–0.75	0.71 0.68–0.75 / 0.86 0.83–0.88	0.78 0.78–0.78 / 0.58 0.58–0.59
CLOCS	0.68 0.65–0.71 / 0.72 0.68–0.75	0.66 0.62–0.70 / 0.83 0.81–0.86	0.75 0.74–0.75 / 0.53 0.53–0.54
MERL	0.75 0.72–0.77 / 0.76 0.73–0.79	0.76 0.72–0.80 / 0.88 0.85–0.90	0.83 0.83–0.83 / 0.66 0.66–0.67
D-BETA	0.72 0.69–0.75 / 0.74 0.71–0.78	0.73 0.70–0.77 / 0.87 0.85–0.89	0.82 0.82–0.82 / 0.64 0.63–0.64

lic benchmarks. MERL achieves the highest AUROC on both mPCWP and mPA, while D-BETA is intermediate and CLOCS is comparable to or below the Random baseline. However, confidence intervals overlap substantially across methods, indicating that any differences are suspect.

5.4.5. PATIENT FORECASTING

On 1-year heart failure forecasting (Table 6), MERL and D-BETA are best and closely matched, outperforming both Random and CLOCS on AUROC and AUPRC. Random also exceeds CLOCS (Δ AUROC = 0.03; Δ AUPRC = 0.05), reinforcing that a randomly initialized encoder is a non-trivial baseline even for patient-level forecasting.

6. Alternative Views

In Section 3 we argue that current downstream evaluation is narrow and should expand to include other clinical targets, such as structural disease, hemodynamic state, and forecasting tasks. A natural concern is that some of these targets cannot admit near-perfect performance due to aleatoric uncertainty, rendering them ill-suited for benchmarking (Ghassemi et al., 2020; Kohane et al., 2021; Pillai et al., 2024;

Yuan et al., 2021). Even so, many influential ML benchmarks have also remained far from saturation, often due to noise and ambiguity, yet have driven progress by rewarding better representations and modeling choices (Northcutt et al., 2021; Vendrow et al., 2025). When an endpoint cannot be perfectly inferred from an ECG, the signal that is present can be clinically meaningful and transferable toward other objectives. Hence, it is important that ECG representations are optimized to capture this information.

A second objection is that many valuable ECG endpoints exist in health systems with non-trivial barriers to public release. However, there is broad precedent in the ML community for benchmarking on hidden test sets, where the data is not released (e.g., Geiger et al., 2012; Wang et al., 2018; Perez Alday et al., 2022). Modern infrastructure enables containerized evaluation where benchmark hosts can run inference on behalf of a participant (Pavao et al., 2023). Private-endpoint benchmarks are especially appropriate for ECG representation learning, where downstream evaluation often tests transferability to tasks unseen during training. To make such benchmarks useful, hosts should publish detailed documentation including cohort and label construction, and provide a transparent auditing pathway when possible. We acknowledge that in practice, data access and requirements will vary across institutions.

7. Discussion

This paper analyzed evaluation of 12-lead ECG representation learning. We proposed a new hierarchy of clinically-grounded tasks, then outlined best-practices, most of which the field fails to follow. Our experiments show that ranking current methods is difficult in practice. They also show the utility of using a randomly initialized encoder as a baseline, since it is surprisingly performant. Future work should explore *why* this is so. We hypothesize that this is because the signal is so apparent in the ECG for many tasks that random convolutions do not distort it.

One limitation of our study is that we focused only on 12-lead ECGs. We expect that our general conclusions hold for pre-trained encoders of other bio-signals (e.g., 1-lead ECG, PPG, and EEG), though this remains to be verified. There is also growing interest in multi-modal representations that include ECG as a component (e.g., Radhakrishnan et al., 2023; Thapa et al., 2024); evaluating such models should be addressed in future studies.

Ultimately, we think the field would benefit from an extensible open-source framework with standardized evaluation code. The community should agree on a core set of clinically important tasks that will drive the future of ECG representation learning.

Acknowledgements

We thank Tiffany Yau for guidance with the hemodynamic inference and patient forecasting tasks. We also thank Danielle Pace and Roey Ringel for helpful discussions and feedback. Zachary Berger is supported by the Department of Defense NDSEG Fellowship. This work was also supported by Quanta Computer Inc.

References

- Al-Masud, M. A., Alcaraz, J. M. L., and Strothoff, N. Benchmarking ecg foundational models: A reality check across clinical tasks, 2025. URL <https://arxiv.org/abs/2509.25095>.
- Bechler-Speicher, M., Finkelshtein, B., Frasca, F., Müller, L., Tönshoff, J., Siraudin, A., Zaverkin, V., Bronstein, M., Niepert, M., Perozzi, B., Galkin, M., and Morris, C. Position: Graph learning will lose relevance due to poor benchmarks. In *Proceedings of the 42nd International Conference on Machine Learning (ICML)*, volume 267 of *Proceedings of Machine Learning Research*, pp. 81067–81089, 2025. URL <https://openreview.net/forum?id=nDFpl21hoH>.
- Bengio, Y., Courville, A., and Vincent, P. Representation learning: A review and new perspectives. *IEEE Trans. Pattern Anal. Mach. Intell.*, 35(8):1798–1828, August 2013. ISSN 0162-8828. doi: 10.1109/TPAMI.2013.50. URL <https://doi.org/10.1109/TPAMI.2013.50>.
- Bergamaschi, T., Yau, T., Chandak, P., Kyereme-Tuah, A., Hung, J., Gaggin, H., Kohane, I. S., and Stultz, C. M. Forecasting left ventricular systolic dysfunction in heart failure with artificial intelligence. *medRxiv*, 2025. doi: 10.1101/2025.04.13.25325744. URL <https://www.medrxiv.org/content/early/2025/04/14/2025.04.13.25325744>.
- Blalock, D. W., Ortiz, J. J. G., Frankle, J., and Guttag, J. V. What is the state of neural network pruning? In Dhillon, I. S., Papailiopoulos, D. S., and Sze, V. (eds.), *Proceedings of the Third Conference on Machine Learning and Systems, MLSys 2020, Austin, TX, USA, March 2-4, 2020*. mlsys.org, 2020.
- Bommasani, R. et al. On the opportunities and risks of foundation models, 2022. URL <https://arxiv.org/abs/2108.07258>.
- Chen, T., Kornblith, S., Norouzi, M., and Hinton, G. A simple framework for contrastive learning of visual representations. In *International conference on machine learning*, pp. 1597–1607. PMLR, 2020.
- Chen, X. and He, K. Exploring simple siamese representation learning. *arXiv preprint arXiv:2011.10566*, 2020.
- Chen, X., Xie, S., and He, K. An empirical study of training self-supervised vision transformers. *arXiv preprint arXiv:2104.02057*, 2021.
- Chen, Y., Orlandi, M., Rapa, P. M., Benatti, S., Benini, L., and Li, Y. Physiowave: A multi-scale wavelet-transformer for physiological signal representation. In *NeurIPS 2025*, 2025. URL <https://openreview.net/forum?id=ayR2JfRYRS>.
- Davis, J. and Goadrich, M. The relationship between precision-recall and roc curves. In *Proceedings of the 23rd International Conference on Machine Learning, ICML '06*, pp. 233–240, New York, NY, USA, 2006. Association for Computing Machinery. ISBN 1595933832. doi: 10.1145/1143844.1143874. URL <https://doi.org/10.1145/1143844.1143874>.
- Devlin, J., Chang, M.-W., Lee, K., and Toutanova, K. BERT: Pre-training of deep bidirectional transformers for language understanding. In Burstein, J., Doran, C., and Solorio, T. (eds.), *Proceedings of the 2019 Conference of the North American Chapter of the Association for Computational Linguistics: Human Language Technologies, Volume 1 (Long and Short Papers)*, pp. 4171–4186, Minneapolis, Minnesota, June 2019. Association for Computational Linguistics. doi: 10.18653/v1/N19-1423. URL <https://aclanthology.org/N19-1423>.
- Diamant, N., Reinertsen, E., Song, S., Aguirre, A. D., Stultz, C. M., and Batra, P. Patient contrastive learning: A performant, expressive, and practical approach to electrocardiogram modeling. *PLOS Computational Biology*, 18(2):e1009862, 2022. doi: 10.1371/journal.pcbi.1009862. URL <https://doi.org/10.1371/journal.pcbi.1009862>.
- Esteva, A., Robicquet, A., Ramsundar, B., Kuleshov, V., DePristo, M., Chou, K., Cui, C., Corrado, G., Thrun, S., and Dean, J. A guide to deep learning in healthcare. *Nature Medicine*, 25(1):24–29, January 2019. doi: 10.1038/s41591-018-0316-z. URL <https://doi.org/10.1038/s41591-018-0316-z>.
- Ferrari Dacrema, M., Cremonesi, P., and Jannach, D. Are we really making much progress? a worrying analysis of recent neural recommendation approaches. In *Proceedings of the 13th ACM Conference on Recommender Systems, RecSys '19*, pp. 101–109, New York, NY, USA, 2019. Association for Computing Machinery. ISBN 9781450362436. doi: 10.1145/3298689.3347058. URL <https://doi.org/10.1145/3298689.3347058>.

- Fisch, C. Centennial of the string galvanometer and the electrocardiogram. *Journal of the American College of Cardiology*, 36(6):1737–1745, 2000. ISSN 0735-1097. doi: [https://doi.org/10.1016/S0735-1097\(00\)00976-1](https://doi.org/10.1016/S0735-1097(00)00976-1). URL <https://www.sciencedirect.com/science/article/pii/S0735109700009761>.
- Friedman, S. F., Khurshid, S., Venn, R. A., Wang, X., Diamant, N., Di Achille, P., Weng, L.-C., Choi, S. H., Reeder, C., Pirruccello, J. P., Singh, P., Lau, E. S., Philip-pakis, A., Anderson, C. D., Maddah, M., Batra, P., Ellinor, P. T., Ho, J. E., and Lubitz, S. A. Unsupervised deep learning of electrocardiograms enables scalable human disease profiling. *npj Digital Medicine*, 8(1):23, 2025. doi: 10.1038/s41746-024-01418-9. URL <https://doi.org/10.1038/s41746-024-01418-9>.
- Fukuta, H. and Little, W. C. The cardiac cycle and the physiologic basis of left ventricular contraction, ejection, relaxation, and filling. *Heart Failure Clinics*, 4(1):1–11, 2008. ISSN 1551-7136. doi: <https://doi.org/10.1016/j.hfc.2007.10.004>. URL <https://www.sciencedirect.com/science/article/pii/S1551713607001377>.
- Diastolic Dysfunction and Heart Failure.
- Gebru, T., Morgenstern, J., Vecchione, B., Vaughan, J. W., Wallach, H., III, H. D., and Crawford, K. Datasheets for datasets. *Commun. ACM*, 64(12):86–92, November 2021. ISSN 0001-0782. doi: 10.1145/3458723. URL <https://doi.org/10.1145/3458723>.
- Geiger, A., Lenz, P., and Urtasun, R. Are we ready for autonomous driving? the kitti vision benchmark suite. In *2012 IEEE Conference on Computer Vision and Pattern Recognition*, pp. 3354–3361, 2012. doi: 10.1109/CVPR.2012.6248074.
- Ghassemi, M., Naumann, T., Schulam, P., Beam, A. L., Chen, I. Y., and Ranganath, R. A review of challenges and opportunities in machine learning for health. *AMIA Joint Summits on Translational Science*, pp. 191–200, May 2020. URL <https://pubmed.ncbi.nlm.nih.gov/32477638/>.
- Goldberger, A. L., Amaral, L. A. N., Glass, L., Hausdorff, J. M., Ivanov, P. C., Mark, R. G., Mietus, J. E., Moody, G. B., Peng, C.-K., and Stanley, H. E. Physiobank, physiotoolkit, and physionet: Components of a new research resource for complex physiologic signals. *Circulation*, 101(23):e215–e220, 2000. doi: 10.1161/01.CIR.101.23.e215. RRID:SCR_007345.
- Gopal, B., Han, R., Raghupathi, G., Ng, A., Tison, G., and Rajpurkar, P. 3kg: Contrastive learning of 12-lead electrocardiograms using physiologically-inspired augmentations. In Roy, S., Pfahl, S., Rocheteau, E., Tadesse, G. A., Oala, L., Falck, F., Zhou, Y., Shen, L., Zamzmi, G., Mugambi, P., Zirikly, A., McDermott, M. B. A., and Alsentzer, E. (eds.), *Proceedings of Machine Learning for Health*, volume 158 of *Proceedings of Machine Learning Research*, pp. 156–167. PMLR, 04 Dec 2021. URL <https://proceedings.mlr.press/v158/gopal21a.html>.
- Gow, B., Pollard, T., Nathanson, L. A., Johnson, A., Moody, B., Fernandes, C., Greenbaum, N., Waks, J. W., Eslami, P., Carbonati, T., Chaudhari, A., Herbst, E., Moukheiber, D., Berkowitz, S., Mark, R., and Horng, S. MIMIC-IV-ECG: Diagnostic electrocardiogram matched subset. <https://physionet.org/content/mimic-iv-ecg/1.0/>, 2023. RRID:SCR_007345.
- Grill, J.-B., Strub, F., Altché, F., Tallec, C., Richemond, P., Buchatskaya, E., Doersch, C., Avila Pires, B., Guo, Z., Gheshlaghi Azar, M., Piot, B., kavukcuoglu, k., Munos, R., and Valko, M. Bootstrap your own latent - a new approach to self-supervised learning. In Larochelle, H., Ranzato, M., Hadsell, R., Balcan, M., and Lin, H. (eds.), *Advances in Neural Information Processing Systems*, volume 33, pp. 21271–21284. Curran Associates, Inc., 2020. URL https://proceedings.neurips.cc/paper_files/paper/2020/file/f3ada80d5c4ee70142b17b8192b2958e-Paper.pdf.
- Han, Y., Murino, V., Liu, X., Zhang, X., and Ding, C. A systematic review on foundation models for electrocardiogram analysis: Initial strides and expansive horizons, 2025. URL <https://arxiv.org/abs/2410.19877>.
- He, H. and Garcia, E. A. Learning from imbalanced data. *IEEE Trans. on Knowl. and Data Eng.*, 21(9):1263–1284, September 2009. ISSN 1041-4347. doi: 10.1109/TKDE.2008.239. URL <https://doi.org/10.1109/TKDE.2008.239>.
- He, K., Zhang, X., Ren, S., and Sun, J. Deep residual learning for image recognition. In *Proceedings of the IEEE Conference on Computer Vision and Pattern Recognition (CVPR)*, June 2016.
- He, K., Chen, X., Xie, S., Li, Y., Dollár, P., and Girshick, R. Masked autoencoders are scalable vision learners, 2021. URL <https://arxiv.org/abs/2111.06377>.
- Herrmann, M., Lange, F. J. D., Eggensperger, K., Casalicchio, G., Wever, M., Feurer, M., Rügamer, D., Hüllermeier, E., Boulesteix, A.-L., and Bischl, B. Position: Why we must rethink empirical research in machine learning. In Salakhutdinov, R., Kolter, Z., Heller, K., Weller, A., Oliver, N., Scarlett, J., and Berkenkamp, F. (eds.), *Proceedings of the 41st International Conference*

- on Machine Learning, volume 235 of *Proceedings of Machine Learning Research*, pp. 18228–18247. PMLR, 21–27 Jul 2024. URL <https://proceedings.mlr.press/v235/herrmann24b.html>.
- Hung, M. P., Saeed, A., and Ma, D. Boosting masked ecg-text auto-encoders as discriminative learners. In *Forty-second International Conference on Machine Learning*, 2024. URL <https://openreview.net/forum?id=mM65b81LdM>.
- Jin, J., Wang, H., Li, H., Li, J., Pan, J., and Hong, S. Reading your heart: Learning ECG words and sentences via pre-training ECG language model. In *The Thirteenth International Conference on Learning Representations*, 2025. URL <https://openreview.net/forum?id=6Hz1Ko087B>.
- Khurshid, S., Friedman, S., Reeder, C., Achille, P. D., Diamant, N., Singh, P., Harrington, L. X., Wang, X., Al-Alusi, M. A., Sarma, G., Foulkes, A. S., Ellinor, P. T., Anderson, C. D., Ho, J. E., Philippakis, A. A., Batra, P., and Lubitz, S. A. Ecg-based deep learning and clinical risk factors to predict atrial fibrillation. *Circulation*, 145(2):122–133, 2022. doi: 10.1161/CIRCULATIONAHA.121.057480. URL <https://www.ahajournals.org/doi/abs/10.1161/CIRCULATIONAHA.121.057480>.
- Kiyasseh, D., Zhu, T., and Clifton, D. A. Clocs: Contrastive learning of cardiac signals across space, time, and patients. In Meila, M. and Zhang, T. (eds.), *Proceedings of the 38th International Conference on Machine Learning*, volume 139 of *Proceedings of Machine Learning Research*, pp. 5606–5615. PMLR, 18–24 Jul 2021. URL <https://proceedings.mlr.press/v139/kiyasseh21a.html>.
- Kohane, I. S., Aronow, B. J., Avillach, P., Beaulieu-Jones, B. K., Bellazzi, R., Bradford, R. L., Brat, G. A., Cannataro, M., Cimino, J. J., García-Barrio, N., Gehlenborg, N., Ghassemi, M., Gutiérrez-Sacristán, A., Hanauer, D. A., Holmes, J. H., Hong, C., Klann, J. G., Loh, N. H. W., Luo, Y., Mandl, K. D., Daniar, M., Moore, J. H., Murphy, S. N., Neuraz, A., Ngiam, K. Y., Omenn, G. S., Palmer, N., Patel, L. P., Pedrera-Jiménez, M., Sliz, P., South, A. M., Tan, A. L. M., Taylor, D. M., Taylor, B. W., Torti, C., Vallejos, A. K., Wagholarikar, K. B., Weber, G. M., and Cai, T. What every reader should know about studies using electronic health record data but may be afraid to ask. *J Med Internet Res*, 23(3):e22219, Mar 2021. ISSN 1438-8871. doi: 10.2196/22219. URL <https://doi.org/10.2196/22219>.
- Koscova, Z., Li, Q., Robichaux, C., Moura Junior, V., Ghanta, M., Gupta, A., Rosand, J., Aguirre, A., Hong, S., Albert, D. E., Xue, J., Parekh, A., Sameni, R., Reyna, M. A., Westover, M. B., and Cliford, G. D. The harvard-emory ecg database. *medRxiv*, 2024. doi: 10.1101/2024.09.27.24314503. URL <https://www.medrxiv.org/content/early/2024/10/01/2024.09.27.24314503>.
- Lai, J., Tan, H., Wang, J., Ji, L., Guo, J., Han, B., Shi, Y., Feng, Q., and Yang, W. Practical intelligent diagnostic algorithm for wearable 12-lead ECG via self-supervised learning on large-scale dataset. *Nature Communications*, 14:3741, 2023. doi: 10.1038/s41467-023-39472-8. URL <https://www.nature.com/articles/s41467-023-39472-8>.
- Lalam, S., Kunderu, H., Ghosh, S., Harish, K., Prasad, A., Lopez-Jimenez, F., Awasthi, S., Attia, Z., Asirvatham, S., Friedman, P., Barve, R., and Babu, M. Ecg representation learning with multi-modal ehr data. *Transactions on Machine Learning Research*, 2023, November 2023. ISSN 2835-8856. Publisher Copyright: © 2023, Transactions on Machine Learning Research. All rights reserved.
- Lan, X., Ng, D., Hong, S., and Feng, M. Intra-inter subject self-supervised learning for multivariate cardiac signals. In *Proceedings of the AAAI Conference on Artificial Intelligence (AAAI-22)*, volume 36, 2022. doi: 10.1609/aaai.v36i4.20376. URL <https://doi.org/10.1609/aaai.v36i4.20376>.
- Le, D., Truong, S., Brijesh, P., Adjero, D. A., and Le, N. scl-st: Supervised contrastive learning with semantic transformations for multiple lead ecg arrhythmia classification. *IEEE Journal of Biomedical and Health Informatics*, 27(6):2818–2828, 2023. doi: 10.1109/JBHI.2023.3246241.
- Li, J., Liu, C., Cheng, S., Arcucci, R., and Hong, S. Frozen language model helps ecg zero-shot learning, 2023. URL <https://arxiv.org/abs/2303.12311>.
- Li, J., Aguirre, A. D., Junior, V. M., Jin, J., Liu, C., Zhong, L., Sun, C., Clifford, G., Brandon Westover, M., and Hong, S. An electrocardiogram foundation model built on over 10 million recordings. *NEJM AI*, 2(7):Aloa2401033, 2025.
- Liao, T., Taori, R., Raji, D., and Schmidt, L. Are we learning yet? a meta review of evaluation failures across machine learning. In Vanschoren, J. and Yeung, S. (eds.), *Proceedings of the Neural Information Processing Systems Track on Datasets and Benchmarks*, volume 1, 2021.
- Lin, T.-Y., Maire, M., Belongie, S., Hays, J., Perona, P., Ramanan, D., Dollár, P., and Zitnick, C. L. Microsoft coco: Common objects in context. In Fleet, D., Pajdla,

- T., Schiele, B., and Tuytelaars, T. (eds.), *Computer Vision – ECCV 2014*, pp. 740–755, Cham, 2014. Springer International Publishing. ISBN 978-3-319-10602-1.
- Lipton, Z. C. and Steinhardt, J. Troubling trends in machine learning scholarship. *ACM Queue*, 17(1), 2019. doi: 10.1145/3317287.3328534. URL <https://doi.org/10.1145/3317287.3328534>.
- Littlejohns, T. J., Holliday, J., Gibson, L. M., Garratt, S., Oesingmann, N., Alfaro-Almagro, F., Bell, J. D., Boultwood, C., Collins, R., Conroy, M. C., et al. The uk biobank imaging enhancement of 100,000 participants: rationale, data collection, management and future directions. *Nature communications*, 11(1):2624, 2020.
- Liu, C., Wan, Z., Cheng, S., Zhang, M., and Arcucci, R. Etp: Learning transferable ecg representations via ecg-text pre-training. In *ICASSP 2024 - 2024 IEEE International Conference on Acoustics, Speech and Signal Processing (ICASSP)*, pp. 8230–8234, 2024a. doi: 10.1109/ICASSP48485.2024.10446742.
- Liu, C., Wan, Z., Ouyang, C., Shah, A., Bai, W., and Arcucci, R. Zero-shot ECG classification with multimodal learning and test-time clinical knowledge enhancement. In Salakhutdinov, R., Kolter, Z., Heller, K., Weller, A., Oliver, N., Scarlett, J., and Berkenkamp, F. (eds.), *Proceedings of the 41st International Conference on Machine Learning*, volume 235 of *Proceedings of Machine Learning Research*, pp. 31949–31963. PMLR, 21–27 Jul 2024b. URL <https://proceedings.mlr.press/v235/liu24bg.html>.
- Liu, F., Liu, C., Zhao, L., Zhang, X., Wu, X., Xu, X., Liu, Y., Ma, C., Wei, S., He, Z., Li, J., and Kwee, E. N. Y. An open access database for evaluating the algorithms of electrocardiogram rhythm and morphology abnormality detection. *Journal of Medical Imaging and Health Informatics*, 8:1368–1373, 2018. doi: 10.1166/jmhi.2018.2442. URL <https://doi.org/10.1166/jmhi.2018.2442>.
- Liu, H., Chen, D., Chen, D., Zhang, X., Li, H., Bian, L., Shu, M., and Wang, Y. A large-scale multi-label 12-lead electrocardiogram database with standardized diagnostic statements. *Scientific Data*, 9:272, 2022. doi: 10.1038/s41597-022-01403-5. URL <https://doi.org/10.1038/s41597-022-01403-5>.
- Liu, Q. and Paparrizos, J. The elephant in the room: Towards a reliable time-series anomaly detection benchmark. In Globerson, A., Mackey, L., Belgrave, D., Fan, A., Paquet, U., Tomczak, J., and Zhang, C. (eds.), *Advances in Neural Information Processing Systems*, volume 37, pp. 108231–108261. Curran Associates, Inc., 2024. doi: 10.52202/079017-3437.
- Lunelli, R., Nicolson, A., Pröll, S. M., Reinstadler, S. J., Bauer, A., and Dlaska, C. Bencheeg and xecg: a benchmark and baseline for ecg foundation models, 2025. URL <https://arxiv.org/abs/2509.10151>.
- McKeen, K., Masood, S., Toma, A., Rubin, B., and Wang, B. Ecg-fm: an open electrocardiogram foundation model. *JAMIA Open*, 8(5):ooaf122, 10 2025. ISSN 2574-2531. doi: 10.1093/jamiaopen/ooaf122. URL <https://doi.org/10.1093/jamiaopen/ooaf122>.
- Mehari, T. and Strothoff, N. Self-supervised representation learning from 12-lead ecg data. *Comput. Biol. Med.*, 141 (C), February 2022. ISSN 0010-4825. doi: 10.1016/j.combiomed.2021.105114. URL <https://doi.org/10.1016/j.combiomed.2021.105114>.
- Moody, B., Hao, S., Gow, B., Pollard, T., Zong, W., and Mark, R. MIMIC-IV Waveform Database. *PhysioNet*, July 2022. doi: 10.13026/a2mw-f949. URL <https://doi.org/10.13026/a2mw-f949>. Version 0.1.0.
- Na, Y., Park, M., Tae, Y., and Joo, S. Guiding masked representation learning to capture spatio-temporal relationship of electrocardiogram. In *International Conference on Learning Representations*, 2024. URL <https://openreview.net/forum?id=WcOohbsF4H>.
- Nerbonne, J. M. and Kass, R. S. Molecular physiology of cardiac repolarization. *Physiological Reviews*, 85(4):1205–1253, 2005. doi: 10.1152/physrev.00002.2005. URL <https://doi.org/10.1152/physrev.00002.2005>. PMID: 16183911.
- Noble, R. J., Hillis, J. S., and Rothbaum, D. A. Electrocardiography. In Walker, H. K., Hall, W. D., and Hurst, J. W. (eds.), *Clinical Methods: The History, Physical, and Laboratory Examinations*, chapter 33. Butterworths, Boston, 3 edition, 1990. URL <https://www.ncbi.nlm.nih.gov/books/NBK354/>.
- Northcutt, C., Athalye, A., and Mueller, J. Pervasive label errors in test sets destabilize machine learning benchmarks. In Vanschoren, J. and Yeung, S. (eds.), *Proceedings of the Neural Information Processing Systems Track on Datasets and Benchmarks*, volume 1, 2021.
- Oh, J., Chung, H., Kwon, J.-m., Hong, D.-g., and Choi, E. Lead-agnostic self-supervised learning for local and global representations of electrocardiogram. In Flores, G., Chen, G. H., Pollard, T., Ho, J. C., and Naumann, T. (eds.), *Proceedings of the Conference on Health, Inference, and Learning*, volume 174 of *Proceedings of Machine Learning Research*, pp. 338–353. PMLR, 07–08 Apr 2022. URL <https://proceedings.mlr.press/v174/oh22a.html>.

- Pavao, A., Guyon, I., Letournel, A.-C., Tran, D.-T., Baro, X., Escalante, H. J., Escalera, S., Thomas, T., and Xu, Z. Codalab competitions: An open source platform to organize scientific challenges. *Journal of Machine Learning Research*, 24(198):1–6, 2023. URL <http://jmlr.org/papers/v24/21-1436.html>.
- Perez Alday, E. A., Gu, A., Shah, A., Liu, C., Sharma, A., Seyedi, S., Bahrami Rad, A., Reyna, M., and Clifford, G. Classification of 12-lead ECGs: The PhysioNet/Computing in cardiology challenge 2020 (version 1.0.2). PhysioNet, 2022. URL <https://doi.org/10.13026/dvyd-kd57>. RRID:SCR_007345.
- Pillai, B., Salerno, M., Schnittger, I., Cheng, S., and Ouyang, D. Precision of echocardiographic measurements. *Journal of the American Society of Echocardiography*, 37(5):562–563, 2024. ISSN 0894-7317. doi: 10.1016/j.echo.2024.01.001. URL <https://doi.org/10.1016/j.echo.2024.01.001>.
- Pineau, J., Vincent-Lamarre, P., Sinha, K., Lariviere, V., Beygelzimer, A., d’Alche Buc, F., Fox, E., and Larochelle, H. Improving reproducibility in machine learning research(a report from the neurips 2019 reproducibility program). *Journal of Machine Learning Research*, 22(164):1–20, 2021. URL <http://jmlr.org/papers/v22/20-303.html>.
- Poterucha, T. J., Jing, L., Ricart, R. P., Adjei-Mosi, M., Finer, J., Hartzel, D., Kelsey, C., Long, A., Rocha, D., Ruhl, J. A., vanMaanen, D., Probst, M. A., Daniels, B., Joshi, S. D., Tastet, O., Corbin, D., Avram, R., Barrios, J. P., Tison, G. H., Chiu, I.-M., Ouyang, D., Volodarskiy, A., Castillo, M., Roedan Oliver, F. A., Malta, P. P., Ye, S., Rosner, G. F., Dizon, J. M., Ali, S. R., Liu, Q., Bradley, C. K., Vaishnav, P., Waksmonski, C. A., DeFilippis, E. M., Agarwal, V., Lebbehn, M., Kampaktsis, P. N., Shames, S., Beecy, A. N., Kumaraiah, D., Homma, S., Schwartz, A., Hahn, R. T., Leon, M., Einstein, A. J., Maurer, M. S., Hartman, H. S., Hughes, J. W., Haggerty, C. M., and Elias, P. Detecting structural heart disease from electrocardiograms using ai. *Nature*, 644:221–230, August 2025. doi: 10.1038/s41586-025-09227-0. URL <https://doi.org/10.1038/s41586-025-09227-0>.
- Radhakrishnan, A., Friedman, S. F., Khurshid, S., Ng, K., Batra, P., Lubitz, S. A., Philippakis, A. A., and Uhler, C. Cross-modal autoencoder framework learns holistic representations of cardiovascular state. *Nature Communications*, 14(1):2436, 2023. doi: 10.1038/s41467-023-38125-0. URL <https://doi.org/10.1038/s41467-023-38125-0>.
- Ribeiro, A. H., Ribeiro, M. H., Paixão, G. M. M., Oliveira, D. M., Gomes, P. R., Canazart, J. A., Ferreira, M. P. S., Andersson, C. R., Macfarlane, P. W., Meira Jr., W., Schön, T. B., and Ribeiro, A. L. P. Automatic diagnosis of the 12-lead ecg using a deep neural network. *Nature Communications*, 11(1):1760, 2020. doi: 10.1038/s41467-020-15432-4.
- Rivera-Ruiz, M., Cajavilca, C., and Varon, J. Einthoven’s string galvanometer. *Texas Heart Institute Journal*, 35(2):174–178, 2008. URL <https://pmc.ncbi.nlm.nih.gov/articles/PMC2435435/>.
- Russakovsky, O., Deng, J., Su, H., Krause, J., Satheesh, S., Ma, S., Huang, Z., Karpathy, A., Khosla, A., Bernstein, M., Berg, A. C., and Fei-Fei, L. ImageNet Large Scale Visual Recognition Challenge. *International Journal of Computer Vision (IJCV)*, 115(3):211–252, 2015. doi: 10.1007/s11263-015-0816-y.
- Saito, T. and Rehmsmeier, M. The precision-recall plot is more informative than the roc plot when evaluating binary classifiers on imbalanced datasets. *PLOS ONE*, 10(3):1–21, 03 2015. doi: 10.1371/journal.pone.0118432. URL <https://doi.org/10.1371/journal.pone.0118432>.
- Schlesinger, D. E., Diamant, N., Raghu, A., Reinertsen, E., Young, K., Batra, P., Pomerantsev, E., and Stultz, C. M. A deep learning model for inferring elevated pulmonary capillary wedge pressures from the 12-lead electrocardiogram. *JACC: Advances*, 1(1):100003, 2022. doi: 10.1016/j.jacadv.2022.100003. URL <https://www.jacc.org/doi/abs/10.1016/j.jacadv.2022.100003>.
- Song, J., Jang, J.-H., Hong, D., myoung Kwon, J., and Jo, Y.-Y. Crema: A contrastive regularized masked autoencoder for robust ecg diagnostics across clinical domains, 2025. URL <https://arxiv.org/abs/2407.07110>.
- Strothoff, N., Wagner, P., Schaeffter, T., and Samek, W. Deep learning for ecg analysis: Benchmarks and insights from ptb-xl. *IEEE Journal of Biomedical and Health Informatics*, 25(5):1519–1528, 2021. doi: 10.1109/JBHI.2020.3022989.
- Sudlow, C., Gallacher, J., Allen, N., Beral, V., Burton, P., Danesh, J., Downey, P., Elliott, P., Green, J., Landray, M., et al. Uk biobank: an open access resource for identifying the causes of a wide range of complex diseases of middle and old age. *PLoS medicine*, 12(3):e1001779, 2015.
- Thapa, R., He, B., Kjaer, M. R., Iv, H. M., Ganjoo, G., Mignot, E., and Zou, J. SleepFM: Multi-modal representation learning for sleep across brain activity, ECG and respiratory signals. In Salakhutdinov, R., Kolter, Z., Heller, K., Weller, A., Oliver, N., Scarlett, J., and Berkenkamp, F. (eds.), *Proceedings of*

- the 41st International Conference on Machine Learning, volume 235 of *Proceedings of Machine Learning Research*, pp. 48019–48037. PMLR, 21–27 Jul 2024. URL <https://proceedings.mlr.press/v235/thapa24a.html>.
- Tian, Y., Li, Z., Jin, Y., Wang, M., Wei, X., Zhao, L., Liu, Y., Liu, J., and Liu, C. Foundation model of ecg diagnosis: Diagnostics and explanations of any form and rhythm on ecg. *Cell Reports Medicine*, 5(12):101875, 2024. URL [https://www.cell.com/cell-reports-medicine/fulltext/S2666-3791\(24\)00646-3](https://www.cell.com/cell-reports-medicine/fulltext/S2666-3791(24)00646-3).
- Vendrow, J., Vendrow, E., Beery, S., and Madry, A. Do large language model benchmarks test reliability?, 2025. URL <https://arxiv.org/abs/2502.03461>.
- Wagner, P., Strothoff, N., Bousseljot, R.-D., Lunze, F. I., Samek, W., and Schaeffter, T. PTB-XL: A large publicly available electrocardiography dataset. *Scientific Data*, 7(1):154, 2020. doi: 10.1038/s41597-020-0495-6.
- Wagner, P., Strothoff, N., Bousseljot, R.-D., Samek, W., and Schaeffter, T. PTB-XL, a large publicly available electrocardiography dataset. <https://physionet.org/content/ptb-xl/1.0.3/>, 2022. RRID:SCR_007345.
- Wan, Z., Yu, Q., Mao, J., Duan, W., and Ding, C. Openecg: Benchmarking ecg foundation models with public 1.2 million records, 2025. URL <https://arxiv.org/abs/2503.00711>.
- Wang, A., Singh, A., Michael, J., Hill, F., Levy, O., and Bowman, S. GLUE: A multi-task benchmark and analysis platform for natural language understanding. In Linzen, T., Chrupala, G., and Alishahi, A. (eds.), *Proceedings of the 2018 EMNLP Workshop BlackboxNLP: Analyzing and Interpreting Neural Networks for NLP*, pp. 353–355, Brussels, Belgium, November 2018. Association for Computational Linguistics. doi: 10.18653/v1/W18-5446. URL <https://aclanthology.org/W18-5446/>.
- Wang, F., Xu, J., and Yu, L. From token to rhythm: A multi-scale approach for ECG-language pretraining. In Singh, A., Fazel, M., Hsu, D., Lacoste-Julien, S., Berkenkamp, F., Maharaj, T., Wagstaff, K., and Zhu, J. (eds.), *Proceedings of the 42nd International Conference on Machine Learning*, volume 267 of *Proceedings of Machine Learning Research*, pp. 65059–65074. PMLR, 13–19 Jul 2025. URL <https://proceedings.mlr.press/v267/wang25du.html>.
- Wang, N., Feng, P., Ge, Z., Zhou, Y., Zhou, B., and Wang, Z. Adversarial spatiotemporal contrastive learning for electrocardiogram signals. *IEEE Transactions on Neural Networks and Learning Systems*, 35(10):13845–13859, 2024. doi: 10.1109/TNNLS.2023.3272153.
- Wei, C. T., Hsieh, M.-E., Liu, C.-L., and Tseng, V. S. Contrastive heartbeats: Contrastive learning for self-supervised ecg representation and phenotyping. In *ICASSP 2022 - 2022 IEEE International Conference on Acoustics, Speech and Signal Processing (ICASSP)*, pp. 1126–1130, 2022. doi: 10.1109/ICASSP43922.2022.9746887.
- Wu, X.-Z. and Zhou, Z.-H. A unified view of multi-label performance measures. In Precup, D. and Teh, Y. W. (eds.), *Proceedings of the 34th International Conference on Machine Learning*, volume 70 of *Proceedings of Machine Learning Research*, pp. 3780–3788. PMLR, 06–11 Aug 2017. URL <https://proceedings.mlr.press/v70/wu17a.html>.
- Yang, C., Westover, M., and Sun, J. Biot: Biosignal transformer for cross-data learning in the wild. In Oh, A., Naumann, T., Globerson, A., Saenko, K., Hardt, M., and Levine, S. (eds.), *Advances in Neural Information Processing Systems*, volume 36, pp. 78240–78260. Curran Associates, Inc., 2023.
- Yu, H., Guo, P., and Sano, A. Ecg semantic integrator (esi): A foundation ecg model pretrained with llm-enhanced cardiological text. *Transactions on Machine Learning Research (TMLR)*, 2024.
- Yuan, N., Jain, I., Rattehalli, N., He, B., Pollick, C., Liang, D., Heidenreich, P., Zou, J., Cheng, S., and Ouyang, D. Systematic quantification of sources of variation in ejection fraction calculation using deep learning. *JACC: Cardiovascular Imaging*, 14(11):2260–2262, 2021. doi: 10.1016/j.jcmg.2021.06.018. URL <https://www.jacc.org/doi/abs/10.1016/j.jcmg.2021.06.018>.
- Zhang, H., Liu, W., Shi, J., Chang, S., Wang, H., He, J., and Huang, Q. Maefe: Masked autoencoders family of electrocardiogram for self-supervised pretraining and transfer learning. *IEEE Transactions on Instrumentation and Measurement*, 72:1–15, 2023a. doi: 10.1109/TIM.2022.3228267.
- Zhang, M.-L. and Zhou, Z.-H. A review on multi-label learning algorithms. *IEEE Transactions on Knowledge and Data Engineering*, 26(8):1819–1837, 2014. doi: 10.1109/TKDE.2013.39.
- Zhang, W., Geng, S., and Hong, S. A simple self-supervised ecg representation learning method via manipulated temporal–spatial reverse detection. *Biomedical Signal Processing and Control*, 79:104194, 2023b. ISSN 1746-8094. doi: <https://doi.org/10.1016/j.bspc.2022.104194>.

URL <https://www.sciencedirect.com/science/article/pii/S1746809422006486>.

Zhang, W., Yang, L., Geng, S., and Hong, S. Self-supervised time series representation learning via cross reconstruction transformer. *IEEE Transactions on Neural Networks and Learning Systems*, 35(11):16129–16138, 2024. doi: 10.1109/TNNLS.2023.3292066.

Zheng, J., Chu, H., Struppa, D., Zhang, J., Yacoub, S. M., El-Askary, H., Chang, A., Ehwerhemuepha, L., Abu-dayyeh, I., Barrett, A., Fu, G., Yao, H., Li, D., Guo, H., and Rakovski, C. Optimal multi-stage arrhythmia classification approach. *Scientific Reports*, 10:2898, 2020. doi: 10.1038/s41598-020-59821-7.

Zheng, J., Guo, H., and Chu, H. A large scale 12-lead electrocardiogram database for arrhythmia study. <https://physionet.org/content/ecg-arrhythmia/1.0.0/>, 2022. RRID:SCR_007345.

Zhou, R., Zhang, Y., and Dong, Y. H-tuning: Toward low-cost and efficient ECG-based cardiovascular disease detection with pre-trained models. In Singh, A., Fazel, M., Hsu, D., Lacoste-Julien, S., Berkenkamp, F., Maharaj, T., Wagstaff, K., and Zhu, J. (eds.), *Proceedings of the 42nd International Conference on Machine Learning*, volume 267 of *Proceedings of Machine Learning Research*, pp. 79548–79569. PMLR, 13–19 Jul 2025. URL <https://proceedings.mlr.press/v267/zhou25aj.html>.

A. Selection of Model Survey Set

We construct a *model survey set* of papers that propose a representation learning method for 12-lead ECGs. In the literature, these are commonly referred to as pre-trained ECG encoders or ECG foundation models.

We consider papers published between January 1, 2019 and December 31, 2025. We begin our survey in 2019 since that date coincides with the invention of contemporary self-supervised and large-scale pretraining methods applied to ECGs, e.g. SimCLR and BYOL (Chen et al., 2020; Grill et al., 2020).

To form the survey set, we first identified methods published in top ML and ML-health venues: ICML, ICLR, NeurIPS, AAAI, CHIL, and ML4H. For each venue, we required that one keyword from each of the following sets appeared in the paper title or abstract:

Cardiac Keyword. ECG, EKG, electrocardiogram, electrocardiography, cardiac, 12-lead, multi-lead, multilead.

Representation Learning Keyword. SSL, self-supervised, contrastive, masked, reconstruction, reconstructive, foundation model, pretrain, pre-train, pre-training, pretraining, multimodal, multi-modal, representation.

If a paper plausibly proposed a transferable 12-lead ECG representation based on its title or abstract, we screened the full text. A paper was included in the survey set if it met the following inclusion criteria:

1. 12-lead ECG is one of the primary modalities considered.
2. The paper proposes a method designed to produce a reusable representation.
3. The paper reports downstream evaluation on at least one 12-lead ECG task using linear probing or fine-tuning.

Because a substantial amount of ECG representation learning work appears outside this ecosystem, we then added any method cited by the initially identified papers in their introduction, related works or as a baseline, provided they fit our inclusion criteria. While this procedure may have missed some relevant papers, e.g., some included in (Han et al., 2025), it has the desirable property of restricting our discussion to work that is directly pertinent to the ML-methods community.

The initial search from the ML venues returned 56 papers, with 11 papers left after screening. There were then an additional 17 cited papers that were included. The resulting survey set contains 28 papers, listed in Table 7. We use this set when making claims about common benchmarking and reporting practices in 12-lead ECG representation learning.

For each method in the survey set, we extracted the following data, which is summarized for each method in Table 8:

- Publication venue.
- Year of publication.
- Pre-training dataset used to develop the representation.
- Downstream datasets the representation is evaluated on.
- Which performance metrics were reported.
- If task-level metrics were reported, or only macro-averaged metrics.
- Whether uncertainty was quantified in the paper.
- If the method compares to a random encoder as a baseline.

Table 7. Selected survey set of 12-lead ECG representation learning methods. For each method we indicate the year and venue of publication, which datasets were used for pre-training, and which datasets were used for downstream evaluation. PhysioNet 2020 includes PTB-XL, CPSC2018, INCART, and G12EC. PhysioNet 2021 includes PTB-XL, CPSC2018, INCART, and G12EC, CSN, and UMich.

Method	Year	Venue	Pretraining Dataset	Evaluation Dataset
CLOCS (Kiyasseh et al., 2021)	2021	ICML	PhysioNet 2020, Chapman	PhysioNet 2020, Chapman, Cardiology, PhysioNet 2017
3KG (Gopal et al., 2021)	2021	ML4H	PhysioNet 2020	PhysioNet 2020
ISL (Lan et al., 2022)	2022	AAAI	PTB-XL, Chapman, CPSC2018	PTB-XL, Chapman, CPSC2018
(Oh et al., 2022)	2022	CHIL	PTB-XL, CPSC2018, G12EC, CSN	PTB-XL, CPSC2018, G12EC
CRT (Zhang et al., 2024)	2022	TNNLS	PTB-XL, HAR, Sleep-EDF	PTB-XL, HAR, Sleep-EDF
CPC (Mehari & Strothoff, 2022)	2022	CIBM	PhysioNet 2020, Chapman, Ribeiro	PTB-XL
PCLR (Diamant et al., 2022)	2022	PLOS-CB	Private Dataset	Private Dataset
CT-HB (Wei et al., 2022)	2022	ICASSP	MIT-BIH, Chapman	MIT-BIH, Chapman, Private Dataset
BIOT (Yang et al., 2023)	2023	NeurIPS	SHHS, PREST, PhysioNet 2020	PTB-XL, CHB-MIT, IIIC Seizure, TUAB, TUEV, HAR
ASTCL (Wang et al., 2024)	2023	TNNLS	PTB-XL, Chapman, CODE, CPSC2018, CMI	PTB-XL, Chapman, CODE, CPSC2018, CMI
sEHR-ECG (Lalam et al., 2023)	2023	TMLR	Private Dataset	PhysioNet 2020, Chapman, Private Dataset
(Lai et al., 2023)	2023	Nat. Comms.	Private Dataset	Private Dataset, CPSC2018
METS (Li et al., 2023)	2023	IDL	PTB-XL	PTB-XL, MIT-BIH
MaeFE (Zhang et al., 2023a)	2023	IEEEETIM	CPSC2018, Ningbo	PTB-XL, CPSC2018
sCL-ST (Le et al., 2023)	2023	IEEEJBHI	CPSC2018, INCART, G12EC, PTB	PTB-XL
T-S Reverse (Zhang et al., 2023b)	2023	BSPC	PhysioNet 2017	PhysioNet 2017
ST-MEM (Na et al., 2024)	2024	ICLR	CSN, CODE-15	PTB-XL, CPSC2018, PhysioNet 2017
ESI (Yu et al., 2024)	2024	TMLR	PTB-XL, MIMIC-IV-ECG, Chapman	PTB-XL, ICBEB
ETP (Liu et al., 2024a)	2024	ICASSP	PTB-XL	PTB-XL and CPSC2018
KED (Tian et al., 2024)	2024	Cell-RM	MIMIC-IV-ECG	CPSC2018, Chapman, G12EC, PTB-XL, Private Dataset
MERL (Liu et al., 2024b)	2024	ICML	MIMIC-IV	PTB-XL, CPSC2018, CSN
D-BETA (Hung et al., 2024)	2025	ICML	MIMIC-IV	PhysioNet 2021, CODE-test
MELP (Wang et al., 2025)	2025	ICML	MIMIC-IV	PTB-XL, CPSC2018, CSN
H-Tuning (Zhou et al., 2025)	2025	ICML	CODE	PTB-XL, CSN, G12EC, Private Dataset
HeartLang (Jin et al., 2025)	2025	ICLR	MIMIC-IV-ECG	PTB-XL, CPSC2018, and Chapman
ECG-FM (McKeen et al., 2025)	2025	JAMIA Open	CPSC2018, PTB-XL, G12EC, CSN, MIMIC-IV	UHN-ECG, MIMIC-IV
ECGFounder (Li et al., 2025)	2025	NEJM-AI	Harvard-Emory ECG Database	PTB-XL, CODE-test, PhysioNet 2017, MIMIC-IV, Private Dataset
CREMA (Song et al., 2025)	2025	CIKM	MIMIC-IV, CODE-15, UKBB, SaMi-Trop, IKEM	PTB-XL

Table 8. Evaluation and reporting choices in our surveyed set of 12-lead ECG representation learning papers. “Y” indicates the practice is clearly reported, and “N” otherwise. The column *per-label* indicates whether the given method reports its results per individual task, or aggregates them together. *UQ* indicates whether the paper uses uncertainty quantification when reporting their results. *Rand* indicates whether the paper compares to a random encoder as a baseline. *AUROC* denotes “area under the receiver operating curve”, *AUPRC* denotes “area under the precision-recall curve”, and *Acc.* denotes “accuracy”.

Method	Metrics Reported	Per-label?	UQ?	Rand?
CLOCS (Kiyasseh et al., 2021)	AUROC	N	Y	Y
3KG (Gopal et al., 2021)	AUROC, F_1	Y	Y	N
ISL (Lan et al., 2022)	AUROC	N	Y	Y
(Oh et al., 2022)	Acc.	N	Y	Y
CRT (Zhang et al., 2024)	AUROC, Acc., F_1	Y	Y	N
CPC (Mehari & Strothoff, 2022)	AUROC	Y	Y	N
PCLR (Diamant et al., 2022)	F_1, R^2	Y	Y	N
CT-HB (Wei et al., 2022)	AUROC, Acc., MCC, Sensitivity, Specificity, PPV	Y	N	N
BIOT (Yang et al., 2023)	AUROC, Acc., AUPRC, F_1	N	Y	N
ASTCL (Wang et al., 2024)	AUROC, F_1	Y	Y	Y
sEHR-ECG (Lalam et al., 2023)	AUROC, AUPRC	Y	Y	Y
(Lai et al., 2023)	AUROC, AUPRC, F_1 , Specificity, Sensitivity, Acc., PPV	Y	N	N
METS (Li et al., 2023)	Acc., PPV, Sensitivity, F_1	N	N	Y
MaeFE (Zhang et al., 2023a)	AUROC, Acc., F_1	Y	N	N
sCL-ST (Le et al., 2023)	AUROC, AUPRC, Acc., F_1, F_2, G_2	Y	N	N
T-S Reverse (Zhang et al., 2023b)	AUROC, Acc., Sensitivity, Specificity	Y	N	N
ST-MEM (Na et al., 2024)	AUROC, F_1 , Acc.	Y	Y	N
ESI (Yu et al., 2024)	AUROC, F_1 , Acc.	N	Y	Y
ETP (Liu et al., 2024a)	AUROC, F_1 , Acc.	Y	N	Y
KED (Tian et al., 2024)	AUROC, AUPRC, Acc., F_1 , MCC, Sensitivity, Specificity	Y	Y	N
MERL (Liu et al., 2024b)	AUROC	N	N	Y
D-BETA (Hung et al., 2024)	AUROC	N	Y	N
MELP (Wang et al., 2025)	AUROC	N	N	N
H-tuning (Zhou et al., 2025)	AUROC, F_2, G_2 , PPV	Y	Y	N
HeartLang (Jin et al., 2025)	AUROC	N	N	N
ECG-FM (McKeen et al., 2025)	AUROC, AUPRC, AUPRG	Y	N	Y
ECGFounder (Li et al., 2025)	AUROC, F_1 , Acc.	Y	Y	N
CREMA (Song et al., 2025)	AUROC, AUPRC	Y	N	Y

B. Datasets

B.1. PTB-XL

PTB-XL (Wagner et al., 2020; 2022) is a dataset of 21,837 12-lead 10-second ECG recordings from 18,885 patients. We follow the field’s conventional benchmarking protocol outlined in (Strothoff et al., 2021).

PTB-XL is often analyzed as four subsets. Each subset has a different number of records, as well as number of associated labels. SUPER includes 21,388 ECGs, SUB includes 21,388 ECGs, RHYTHM includes 21,030 ECGs, and FORM includes 8,978 ECGs. For each subset, we detail the prevalence and total number of positive examples of each label in each split in the following tables: SUPER (Table 9), SUB (Table 10), RHYTHM (Table 11), and FORM (Table 12).

Table 9. Downstream tasks with their definition in PTB-XL SUPER. For each label, we report the prevalence of the positive class in the whole dataset. We then report the total number of positive examples in the train, validation, and test set after splitting.

Task	Description	Prevalence (%)	N Train	N Val	N Test
CD	Conduction Disturbance	22.90%	3907	495	496
HYP	Hypertrophy	12.39%	2119	268	262
MI	Myocardial Infarction	25.57%	4379	540	550
NORM	Normal ECG	44.48%	7596	955	963
STTC	ST/T Change	24.48%	4186	528	521

Table 10. Downstream tasks with their definition in PTB-XL SUB. For each label, we report the prevalence of the positive class in the whole dataset. We then report the total number of positive examples in the train, validation, and test set after splitting.

Task	Description	Prevalence (%)	N Train	N Val	N Test
AMI	Anterior myocardial infarction	14.39%	2466	306	306
CLBBB	Complete left bundle branch block	2.51%	428	54	54
CRBBB	Complete right bundle branch block	2.53%	432	55	54
ILBBB	Incomplete left bundle branch block	0.36%	62	7	8
IMI	Inferior myocardial infarction	15.29%	2618	326	327
IRBBB	Incomplete right bundle branch block	5.23%	894	112	112
ISCA	Ischemic in lateral leads	4.40%	756	92	93
ISCI	Ischemic in inferolateral leads	1.86%	318	39	40
ISC ₋	Non-specific ischemic	5.95%	1019	125	128
IVCD	Non-specific intraventricular conduction disturbance (block)	3.68%	630	78	79
LAFB/LPFB	Left anterior/posterior fascicular block	8.40%	1437	181	179
LAO/LAE	Left atrial overload/enlargement	1.99%	341	43	42
LMI	Lateral myocardial infarction	0.94%	161	20	20
LVH	Left ventricular hypertrophy	9.97%	1708	210	214
NORM	Normal ECG	44.48%	7596	955	963
NST ₋	Non-specific ST changes	3.59%	615	75	77
PMI	Posterior myocardial infarction	0.08%	13	2	2
RAO/RAE	Right atrial overload/enlargement	0.46%	79	10	10
RVH	Right ventricular hypertrophy	0.59%	102	12	12
SEHYP	Septal hypertrophy	0.14%	24	3	2
STTC	ST/T Change	10.47%	1792	225	222
WPW	Wolf-Parkinson-White syndrome	0.37%	64	7	8
AVB	AV block	3.85%	658	83	82

Position: Evaluation of ECG Representations Must Be Fixed

Table 11. Downstream tasks with their definition in PTB-XL RHYTHM. For each label, we report the prevalence of the positive class in the whole dataset. We then report the total number of positive examples in the train, validation, and test set after splitting.

Task	Description	Prevalence (%)	N Train	N Val	N Test
AFIB	Atrial fibrillation	7.20%	1211	151	152
AFLT	Atrial flutter	0.35%	59	7	7
BIGU	Bigeminal pattern (unknown origin, SV or Ventricular)	0.39%	66	8	8
PACE	Normal functioning artificial pacemaker	1.40%	237	29	28
PSVT	Paroxysmal supraventricular tachycardia	0.11%	19	3	2
SARRH	Sinus arrhythmia	3.67%	618	77	77
SBRAD	Sinus bradycardia	3.03%	509	64	64
SR	Sinus rhythm	79.64%	13404	1670	1674
STACH	Sinus tachycardia	3.93%	661	83	82
SVARR	Supraventricular arrhythmia	0.75%	128	15	14
SVTAC	Supraventricular tachycardia	0.13%	21	3	3
TRIGU	Trigeminal pattern (unknown origin, SV or Ventricular)	0.10%	16	2	2

Table 12. Downstream tasks with their definition in PTB-XL FORM. For each label, we report the prevalence of the positive class in the whole dataset. We then report the total number of positive examples in the train, validation, and test set after splitting.

Task	Description	Prevalence (%)	N Train	N Val	N Test
ABQRS	Abnormal QRS	37.06%	2683	322	322
DIG	Digitalis-effect	2.02%	145	18	18
HVOLT	High QRS voltage	0.69%	49	7	6
INVT	Inverted T-waves	3.27%	235	30	29
LNGQT	Long QT-interval	1.30%	94	12	11
LOWT	Low amplitude T-waves	4.88%	350	44	44
LPR	Prolonged PR interval	3.79%	272	34	34
LVOLT	Low QRS voltages in the frontal and horizontal leads	2.03%	145	19	18
NDT	Non-diagnostic T abnormalities	20.33%	1461	182	182
NST_	Non-specific ST changes	8.54%	615	75	77
NT_	Non-specific T-wave changes	4.71%	340	41	42
PAC	Atrial premature complex	4.43%	318	40	40
PRC(S)	Premature complex(es)	0.11%	8	1	1
PVC	Ventricular premature complex	12.73%	915	114	114
QWAVE	Q waves present	6.10%	438	55	55
STD_	Non-specific ST depression	11.24%	807	101	101
STE_	Non-specific ST elevation	0.31%	22	3	3
TAB_	T-wave abnormality	0.39%	28	4	3
VCLVH	Voltage criteria (QRS) for left ventricular hypertrophy	9.75%	701	87	87

B.2. CPSC2018

The China Physiological Signal Challenge 2018 (CPSC2018) (Liu et al., 2018) is a dataset of 6,877 ECGs sampled at 500 Hz. Recording duration varies between 5 and 72 seconds. We exclude recordings shorter than 10 seconds, and for longer recordings, clip them to 10 seconds. We are left with 6,867 ECGs used for downstream evaluation.

The dataset is multi-label with 9 tasks. The prevalence and total number of positive examples for each split is reported in Table 13.

Table 13. Downstream tasks with their definition in CPSC2018. For each label, we report the prevalence of the positive class in the whole dataset. We then report the total number of positive examples in the train, validation, and test set after splitting.

Task	Description	Prevalence (%)	N Train	N Val	N Test
AF	Atrial fibrillation	17.77%	852	134	234
IAVB	1st degree AV block	10.50%	494	79	148
LBBB	Left bundle branch block	3.42%	162	27	46
NSR	Sinus rhythm	13.37%	647	81	190
PAC	Premature atrial contraction	8.94%	441	55	118
PVC	Premature ventricular contractions	10.18%	482	71	146
RBBB	Right bundle branch block	27.00%	1282	202	370
STD	ST depression	12.64%	617	87	164
STE	ST elevation	3.20%	155	15	50

B.3. CSN

The Chapman-Shaoxing-Ningbo (CSN) database (Zheng et al., 2020) is a dataset of 45,152 10-second, 12-lead ECG recordings from 10,646 patients sampled at 500 Hz. CSN is a multi-label dataset with 63 diagnostic labels. We restrict our experiments to 48 labels, excluding 13 that have no positive examples in the dataset (2AVB2, AVNRT, IDC, LBBB, LBBB, LVQRSCL, LVQRSLL, MI, MIBW, MIFW, MILW, SAAWR, WAVN) and 2 that have fewer than three positive examples (3AVB, ABI). Diagnostic labels are derived from routine clinical interpretations.

We remove ECGs containing a diagnostic code that is not found in the database's code map, resulting in 31,898 recordings used for downstream evaluation.

ECG recordings are randomly split at the record level into training, validation, and test sets with a ratio of 70/10/20. We note that this dataset did not include associated patient ID with each record to enable a patient-level split. The prevalence of the remaining labels, along with the number of positive examples in each split, is reported in Table 14.

Position: Evaluation of ECG Representations Must Be Fixed

Table 14. Downstream tasks with their definition in CSN. For each label, we report the prevalence of the positive class in the whole dataset. We then report the total number of positive examples in the train, validation, and test set after splitting.

Task	Description	Prevalence (%)	N Train	N Val	N Test
1AVB	1 degree atrioventricular block	2.19%	490	66	144
2AVB	2 degree atrioventricular block	0.07%	14	4	4
2AVB1	2 degree atrioventricular block(Type one)	0.05%	10	3	3
AF	Atrial Flutter	10.46%	2344	292	700
AFIB	Atrial Fibrillation	4.43%	981	136	296
ALS	Axis left shift	2.89%	648	84	189
APB	Atrial premature beats	2.14%	471	61	152
AQW	Abnormal Q wave	1.85%	423	52	115
ARS	Axis right shift	1.66%	365	52	114
AT	Atrial Tachycardia	0.54%	104	20	48
AVB	Atrioventricular block	0.55%	116	15	45
AVRT	Atrioventricular Reentrant Tachycardia	0.02%	3	1	3
CCR	Counterclockwise rotation	0.44%	106	7	28
CR	Clockwise rotation	0.24%	49	8	18
ERV	Early repolarization of the ventricles	0.83%	180	33	53
FQRS	FQRS Wave	0.01%	1	1	1
IVB	Intraventricular block	1.35%	288	42	99
JEB	Junctional escape beat	0.08%	17	3	4
JPT	Junctional premature beat	0.02%	5	1	1
LFBBB	Left front bundle branch block	0.66%	146	23	40
LVH	Left ventricular hypertrophy	0.35%	78	8	27
LVQRSAL	Lower voltage QRS in all leads	2.35%	533	85	131
MISW	Myocardial infarction in the side wall	0.17%	44	5	6
PRIE	PR interval extension	0.09%	22	2	5
PWC	P wave Change	0.27%	62	7	18
QTIE	QT interval extension	0.58%	138	16	31
RAH	Right atrial hypertrophy	0.02%	4	1	1
RBBB	Right bundle branch block	1.67%	363	58	112
RVH	Right ventricle hypertrophy	0.09%	21	1	7
SA	Sinus Irregularity	6.56%	1444	203	446
SB	Sinus Bradycardia	40.16%	8951	1324	2535
SR	Sinus Rhythm	22.31%	5020	720	1375
ST	Sinus Tachycardia	16.11%	3583	507	1049
STDD	ST drop down	1.34%	289	36	102
STE	ST extension	1.30%	288	46	81
STTC	ST-T Change	2.75%	605	83	188
STTU	ST tilt up	0.46%	106	9	32
SVT	Supraventricular Tachycardia	1.92%	432	63	118
TWC	T wave Change	14.55%	3226	466	948
TWO	T wave opposite	3.51%	803	97	219
UW	U wave	0.18%	42	5	11
VB	Ventricular bigeminy	0.01%	1	1	1
VEB	Ventricular escape beat	0.07%	10	4	7
VET	Ventricular escape trigeminy	0.02%	3	2	2
VFW	Ventricular fusion wave	0.03%	2	2	5
VPB	Ventricular premature beat	0.74%	174	20	43
VPE	Ventricular preexcitation	0.04%	7	2	3
WPW	Wolff Parkinson White Pattern	0.17%	41	4	8

B.4. EchoNext

EchoNext (Poterucha et al., 2025) is a dataset collected at Columbia University Irving Medical Center of 100,000 10-second ECGs with labels derived from contemporaneous echocardiograms. The dataset includes both continuous measurements and binarized labels, the latter of which we focus on in our experiments.

All ECGs were natively sampled at 250 Hz; we linearly interpolate them to 500 Hz. All ECGs in the dataset were z-scored using dataset statistics. The upper 99.9-th and lower 0.1-st percentile of voltages was clipped. The dataset mean and standard deviation were saved, which we use to re-scale all examples back to millivolts.

EchoNext recommends a standard split into four mutually exclusive subsets: train, validation, test, and no_split. The no_split subset is treated as a hold-out set. In our experiments, we use the train, validation, and test sets, which amounts to 82,543 samples. The training set, which includes 72,475 examples, represents 26,218 patients, so includes more than one ECG per patient. However, the validation and test sets, which contain 4,626 and 5,442 examples respectively, only contain the latest ECG per patient.

Table 15 contains a list of all binary labels in the EchoNext dataset. We list the prevalence for each label, as well as the total number of positive examples represented in the train, validation, and test sets. We use standard abbreviations for each task. We note that SHD is a binary label indicating any moderate or severe structural abnormality as defined by meeting the threshold for any of the other labels in this table.

Table 15. Downstream tasks with their definition in EchoNext. For each label, we report the prevalence of the positive class in the whole dataset. We then report the total number of positive examples in the train, validation, and test set after splitting.

Task	Description	Prevalence (%)	N Train	N Val	N Test
AR	Moderate or severe aortic regurgitation	1.22	878	62	66
AS	Moderate or severe aortic stenosis	4.19	2919	252	286
LVEF \leq 45	Left ventricular ejection fraction is $\leq 45\%$	22.76	16962	866	962
LVWT \geq 13	Maximum of interventricular septum or posterior wall is ≥ 1.3 cm	23.75	17667	877	1061
MR	Moderate or severe mitral regurgitation	8.18	6137	282	337
PASP \geq 45	Pulmonary artery systolic pressure is ≥ 45 mmHg	18.18	13727	581	699
PEFF	Presence of a moderate or large pericardial effusion	2.67	2079	52	69
PR	Moderate or severe pulmonary regurgitation	0.78	603	21	20
RVSD	Moderate or severe right ventricular systolic dysfunction	12.58	9597	368	419
SHD	Any moderate or severe structural heart disease	51.20	37958	1990	2318
TR-MAX \geq 32	Maximum tricuspid regurgitation velocity is ≥ 3.2 m/s	9.85	7492	267	375
TR	Moderate or severe tricuspid regurgitation	10.13	7707	305	353

B.5. Hemodynamic Inference

For hemodynamic inference we use a private dataset of 9,226 10-second 12-lead ECGs collected from 5,072 patients at Massachusetts General Hospital (MGH), originally introduced by (Schlesinger et al., 2022). Each ECG is paired with contemporaneous invasive hemodynamic measurements obtained via right heart catheterization, which serve as ground-truth labels.

We consider two binary classification tasks: inferring elevated mean pulmonary capillary wedge pressure (mPCWP) and elevated mean pulmonary artery pressure (mPA). Measurements are binarized with $mPCWP \geq 15$ mmHg and $mPA \geq 20$ mmHg indicating a positive label.

We construct patient-level splits to avoid information leakage across sets. Patients are randomly divided into training (70%), validation (10%), and test (20%) cohorts. The training set may contain multiple ECGs per patient. We only retain one ECG per patient in the validation and test set; if multiple ECGs are present for a given patient, then a single ECG is selected uniformly at random.

After processing, we are left with 6,458 examples in the training set, 507 in the validation set, and 1,015 in the test set. Table 16 summarizes the two downstream hemodynamic inference tasks, including label definitions, overall prevalence, and the number of positive examples in each split.

Table 16. Downstream hemodynamic inference tasks. For each binary label, we report the prevalence of the positive class in the full dataset, as well as the number of positive examples in the train, validation, and test sets.

Task	Description	Prevalence (%)	N Train	N Val	N Test
mPA	Mean pulmonary arterial pressure ≥ 20 mmHg measured by right heart catheterization	68.16	4,297	389	753
mPCWP	Mean pulmonary capillary wedge pressure ≥ 15 mmHg measured by right heart catheterization	49.30	3,066	303	565

B.6. Patient Forecasting

For patient forecasting we evaluate on the risk of developing heart failure within 1 year of an ECG (1YR-HF). In particular, we frame this as a binary prediction task with the outcome defined with echocardiographic ground truth as a left ventricular ejection fraction (LVEF) below 40%. We rely on a private longitudinal dataset collected at Massachusetts General Hospital (MGH), originally introduced by (Bergamaschi et al., 2025). The full dataset contains 913,420 10-second 12-lead ECGs from 82,244 patients and is designed to support long-term outcome prediction from ECGs. After filtering examples that have data for the given task, and those with NaN or Inf values, we are left with 426,081 ECGs from 46,694 patients.

We use patient-level data splits following the original dataset construction, assigning all ECGs from a given patient to the same split to prevent information leakage across sets. Patients are split into training (75%), validation (10%), and test (15%) cohorts, with all ECGs from a given patient assigned to the same split. Table 17 summarizes the patient forecasting task, including the label definition, prevalence, and number of positive examples in each split.

Table 17. Patient forecasting task. For the binary outcome, we report the prevalence of the positive class in the full dataset, as well as the number of positive examples in the train, validation, and test sets.

Task	Description	Prevalence (%)	N Train	N Val	N Test
1YR-HF	Development of heart failure within one year, defined as left ventricular ejection fraction $< 40\%$ on an echocardiogram	29.49	93,960	12,929	18,774

C. Training Details

C.1. Linear Probing

To evaluate the quality of learned representations, we freeze each encoder then perform linear probing on the embeddings. We train a separate ℓ_2 -regularized logistic regression model for each label. For our implementation we use `scikit-learn`.

For a given task, we select hyperparameters via a grid search on the validation set. The sweep considers three hyperparameters: feature standardization, the inverse regularization strength, and class weighting:

1. The `scale` hyperparameter controls whether feature standardization is applied. When enabled, each embedding dimension is rescaled to zero mean and unit variance using statistics computed on the training set only.
2. The inverse regularization strength C controls the strength of ℓ_2 regularization in the logistic regression classifier. Smaller values of C correspond to stronger regularization, while larger values allow the classifier to fit the training data more closely.
3. The `class_weight` hyperparameter determines how class imbalance is handled during training. When set to `balanced`, class weights are assigned inversely proportional to class frequencies in the training data. Otherwise, all classes are weighted equally.

The hyperparameter grid we swept over is as follows:

$$\text{scale} \in \{\text{True}, \text{False}\}, \quad C \in \{0.01, 0.1, 1.0, 10.0\}, \quad \text{class_weight} \in \{\text{None}, \text{balanced}\}.$$

All models are trained to convergence with a maximum of 10,000 optimization iterations. The best-performing configuration is selected based on validation loss and is evaluated once on the held-out test set.

C.2. CLOCS

Background. CLOCS (Kiyasseh et al., 2021) is a popular ECG-specific self-supervised learning approach that constructs contrastive pairs directly from the temporal structure and lead organization of ECG signals. We use the publicly available CLOCS implementation repository and make several modifications, all of which will be open-sourced in our code release.

CLOCS defines a family of contrastive objectives, including contrastive multi-segment coding (CMSC), contrastive multi-lead coding (CMLC), and contrastive multi-segment multi-lead coding (CMSMLC). CMSC constructs positive pairs by sampling multiple temporal segments from the same ECG recording, encouraging representations to be invariant to temporal cropping. CMLC instead constructs positive pairs across different leads of the same ECG, encouraging invariance across lead views. CMSMLC combines both objectives by simultaneously contrasting multiple temporal segments and multiple leads from the same ECG. In the original CLOCS paper, CMSC is reported to achieve the strongest average performance across downstream tasks, and we therefore focus on CMSC for comparison.

In the released CLOCS code-base, CMSC is implemented only for single-lead ECGs. To support 12-lead ECG pre-training, we extend this objective by treating each lead as a separate channel, consistent with the approach of (Oh et al., 2022).

Formulation. Given a 10-second ECG recording $\mathbf{x} \in \mathbb{R}^{12 \times T}$, where T is the number of samples, we select two non-overlapping 5-second temporal segments $\mathbf{x}^{(1)}$ and $\mathbf{x}^{(2)}$ from the same recording. Each segment is encoded using a shared encoder network, producing ℓ_2 -normalized embeddings $\tilde{\mathbf{z}}^{(1)}, \tilde{\mathbf{z}}^{(2)} \in \mathbb{R}^E$, where E is the embedding dimension.

Given a mini-batch of B ECG recordings, we define the cosine similarity between embeddings with temperature τ as

$$s_{ij} = \frac{(\tilde{\mathbf{z}}_i^{(1)})^\top \tilde{\mathbf{z}}_j^{(2)}}{\tau}.$$

Segments originating from the same ECG form positive pairs, while segments from different ECGs in the batch serve as negative pairs. We optimize a symmetric InfoNCE objective:

$$\mathcal{L} = -\frac{1}{2B} \sum_{i=1}^B \left[\log \frac{\exp(s_{ii})}{\sum_{j=1}^B \exp(s_{ij})} + \log \frac{\exp(s_{ii})}{\sum_{j=1}^B \exp(s_{ji})} \right].$$

Training. Pre-training is performed on raw 10-second ECG recordings sampled at 500 Hz from the MIMIC-IV dataset, after removing ECGs containing `NaN` or `Inf` values. The resulting dataset is split into training and validation sets using a 90/10 split, corresponding to 719,394 ECGs for training and 80,641 ECGs for validation. The final model checkpoint is selected based on the minimum validation contrastive loss. Models are trained for 50 epochs, corresponding to a comparable number of optimization steps as used in MERL and D-BETA.

We use the same encoder architecture as CLOCS and train using Adam optimization. The original CLOCS paper does not report a hyperparameter grid search and instead fixes the learning rate to 10^{-4} , the temperature to $\tau = 0.1$, and the batch size to 256. We adopt the same batch size and temperature, and perform a grid search over learning rates $\{10^{-3}, 10^{-4}, 10^{-5}\}$ using the validation set. Based on validation loss, we ultimately selected the model trained with a learning rate of 10^{-4} . We do not apply signal perturbations during pre-training, as the main results in the CLOCS paper are reported without perturbations.

Evaluation Protocol. CLOCS operates on 5-second ECG segments during pre-training, while the downstream evaluation datasets contain 10-second ECG recordings. At evaluation time, we split each 10-second ECG recording \mathbf{x} into two non-overlapping 5-second segments, $\mathbf{x}^{(1)}$ and $\mathbf{x}^{(2)}$. Each 5-second segment is independently encoded, and those embeddings are used to train a logistic regression classifier, producing class probability vectors $\mathbf{p}^{(1)}$ and $\mathbf{p}^{(2)}$. The final prediction is obtained by averaging the two probability vectors:

$$\mathbf{p} = \frac{1}{2} \left(\mathbf{p}^{(1)} + \mathbf{p}^{(2)} \right).$$

D. Complete Evaluation on PTB-XL

In Appendix D.1 we show the AUROC and AUPRC for every task within each of the four PTB-XL datasets.

In Appendix D.2 we show the macro-AUROC on PTB-XL SUB, RHYTHM, FORM before and after removing tasks with fewer than 10 positive labels in the test set. We do not show a table for SUPER since each task has far more than 10 positive labels in the test set.

D.1. Performance On Standard Splits

Table 18. Performance for every task in PTB-XL SUPER. Each cell reports AUROC (top line) and AUPRC (bottom line) with 95% confidence intervals.

Task	Random	CLOCS	MERL	D-BETA
CD	0.844 0.822–0.865 / 0.720 0.682–0.751	0.793 0.768–0.816 / 0.623 0.583–0.665	0.893 0.875–0.909 / 0.790 0.759–0.819	0.902 0.885–0.918 / 0.812 0.784–0.838
HYP	0.847 0.816–0.872 / 0.545 0.488–0.601	0.845 0.817–0.871 / 0.539 0.478–0.596	0.883 0.859–0.905 / 0.608 0.552–0.663	0.811 0.785–0.838 / 0.437 0.381–0.495
MI	0.844 0.825–0.862 / 0.650 0.611–0.688	0.744 0.719–0.768 / 0.561 0.523–0.598	0.889 0.873–0.905 / 0.779 0.748–0.808	0.906 0.891–0.921 / 0.814 0.785–0.839
NORM	0.891 0.877–0.904 / 0.838 0.812–0.862	0.859 0.843–0.874 / 0.788 0.761–0.813	0.926 0.916–0.937 / 0.884 0.861–0.904	0.930 0.920–0.940 / 0.895 0.876–0.912
STTC	0.879 0.863–0.895 / 0.689 0.650–0.727	0.866 0.847–0.882 / 0.686 0.647–0.723	0.924 0.911–0.935 / 0.793 0.760–0.826	0.915 0.901–0.928 / 0.783 0.746–0.816

Table 19. Performance for every task in PTB-XL SUB. Each cell reports AUROC (top line) and AUPRC (bottom line) with 95% confidence intervals.

Task	Random	CLOCS	MERL	D-BETA
AMI	0.891 0.871–0.910 / 0.605 0.553–0.661	0.855 0.830–0.879 / 0.576 0.522–0.628	0.957 0.946–0.967 / 0.833 0.799–0.865	0.954 0.941–0.966 / 0.824 0.782–0.863
CLBBB	0.994 0.989–0.998 / 0.855 0.748–0.940	0.982 0.968–0.990 / 0.642 0.522–0.764	0.999 0.997–1.000 / 0.938 0.877–0.984	0.999 0.997–1.000 / 0.969 0.932–0.996
CRBBB	0.993 0.989–0.996 / 0.787 0.684–0.878	0.982 0.970–0.991 / 0.698 0.576–0.813	0.998 0.997–0.999 / 0.890 0.777–0.979	0.997 0.995–0.998 / 0.823 0.718–0.925
ILBBB	0.872 0.658–0.990 / 0.154 0.045–0.345	0.894 0.744–0.980 / 0.120 0.031–0.307	0.883 0.676–0.992 / 0.152 0.061–0.315	0.928 0.798–0.996 / 0.281 0.101–0.567
IMI	0.857 0.835–0.877 / 0.521 0.470–0.572	0.675 0.644–0.706 / 0.304 0.263–0.352	0.837 0.813–0.859 / 0.517 0.464–0.569	0.897 0.880–0.914 / 0.691 0.646–0.734
IRBBB	0.856 0.817–0.893 / 0.298 0.231–0.373	0.816 0.776–0.853 / 0.210 0.163–0.271	0.968 0.958–0.977 / 0.640 0.554–0.722	0.931 0.908–0.949 / 0.485 0.406–0.575
ISCA	0.804 0.764–0.840 / 0.160 0.114–0.215	0.862 0.829–0.895 / 0.214 0.161–0.282	0.913 0.890–0.935 / 0.320 0.246–0.402	0.918 0.899–0.934 / 0.253 0.204–0.317
ISCI	0.852 0.797–0.902 / 0.181 0.097–0.291	0.734 0.662–0.805 / 0.091 0.037–0.171	0.842 0.771–0.908 / 0.270 0.143–0.415	0.922 0.892–0.949 / 0.234 0.143–0.360
ISC ₋	0.918 0.888–0.945 / 0.528 0.443–0.612	0.926 0.901–0.947 / 0.501 0.424–0.584	0.953 0.931–0.970 / 0.647 0.565–0.723	0.935 0.914–0.953 / 0.523 0.444–0.607
IVCD	0.688 0.626–0.744 / 0.110 0.070–0.162	0.630 0.564–0.695 / 0.075 0.051–0.115	0.754 0.686–0.814 / 0.174 0.117–0.248	0.731 0.673–0.790 / 0.142 0.092–0.209
LAFB/LPFB	0.943 0.921–0.963 / 0.723 0.658–0.784	0.863 0.833–0.890 / 0.424 0.357–0.493	0.916 0.895–0.933 / 0.573 0.506–0.640	0.953 0.933–0.969 / 0.765 0.709–0.819
LAO/LAE	0.737 0.670–0.798 / 0.044 0.033–0.058	0.655 0.568–0.734 / 0.042 0.028–0.065	0.839 0.777–0.890 / 0.143 0.083–0.227	0.821 0.760–0.874 / 0.105 0.062–0.168
LMI	0.804 0.693–0.899 / 0.087 0.035–0.173	0.683 0.574–0.786 / 0.022 0.013–0.035	0.761 0.669–0.844 / 0.027 0.017–0.041	0.689 0.589–0.772 / 0.019 0.013–0.033
LVH	0.924 0.907–0.941 / 0.631 0.569–0.694	0.910 0.889–0.929 / 0.588 0.525–0.649	0.930 0.912–0.945 / 0.665 0.604–0.720	0.859 0.835–0.882 / 0.455 0.389–0.523
NORM	0.888 0.874–0.901 / 0.835 0.811–0.860	0.858 0.843–0.873 / 0.786 0.760–0.812	0.922 0.910–0.933 / 0.876 0.853–0.898	0.929 0.918–0.939 / 0.894 0.875–0.912
NST ₋	0.734 0.685–0.782 / 0.121 0.079–0.185	0.731 0.672–0.787 / 0.145 0.091–0.223	0.850 0.808–0.887 / 0.186 0.135–0.256	0.827 0.777–0.869 / 0.227 0.153–0.312
PMI	0.480 0.136–0.842 / 0.003 0.001–0.006	0.410 0.205–0.624 / 0.001 0.001–0.002	0.935 0.867–0.998 / 0.097 0.007–0.333	0.848 0.735–0.962 / 0.009 0.003–0.024
RAO/RAE	0.844 0.724–0.947 / 0.035 0.017–0.066	0.705 0.520–0.884 / 0.022 0.008–0.048	0.955 0.912–0.991 / 0.210 0.078–0.411	0.858 0.737–0.960 / 0.170 0.022–0.425
RVH	0.884 0.764–0.974 / 0.261 0.072–0.535	0.889 0.720–0.986 / 0.272 0.093–0.489	0.863 0.697–0.990 / 0.373 0.127–0.660	0.957 0.912–0.986 / 0.178 0.074–0.367
SEHYP	0.976 0.961–0.990 / 0.040 0.023–0.087	0.611 0.297–0.929 / 0.005 0.001–0.013	0.882 0.800–0.959 / 0.010 0.005–0.022	0.922 0.909–0.935 / 0.010 0.008–0.014
STTC	0.820 0.794–0.845 / 0.307 0.263–0.355	0.820 0.792–0.845 / 0.311 0.269–0.357	0.881 0.862–0.900 / 0.451 0.392–0.514	0.859 0.834–0.883 / 0.423 0.369–0.488
WPW	0.769 0.605–0.925 / 0.071 0.008–0.245	0.790 0.587–0.933 / 0.026 0.009–0.060	0.960 0.881–0.998 / 0.521 0.222–0.824	0.841 0.671–0.972 / 0.489 0.135–0.849
AVB	0.739 0.674–0.798 / 0.110 0.079–0.151	0.705 0.642–0.765 / 0.121 0.080–0.184	0.962 0.948–0.975 / 0.569 0.467–0.662	0.972 0.963–0.980 / 0.571 0.470–0.675

Table 20. Performance for every task in PTB-XL RHYTHM. Each cell reports AUROC (top line) and AUPRC (bottom line) with 95% confidence intervals.

Task	Random	CLOCS	MERL	D-BETA
AFIB	0.857 0.824–0.886 / 0.371 0.305–0.446	0.832 0.798–0.861 / 0.331 0.266–0.397	0.978 0.964–0.989 / 0.833 0.764–0.898	0.987 0.973–0.997 / 0.952 0.920–0.977
AFLT	0.818 0.657–0.991 / 0.183 0.018–0.467	0.900 0.749–0.993 / 0.274 0.050–0.652	0.952 0.854–1.000 / 0.661 0.326–0.934	0.959 0.874–1.000 / 0.750 0.423–1.000
BIGU	0.627 0.366–0.882 / 0.095 0.015–0.253	0.777 0.609–0.913 / 0.262 0.008–0.628	0.716 0.490–0.924 / 0.122 0.017–0.347	0.977 0.960–0.993 / 0.303 0.082–0.598
PACE	0.851 0.734–0.942 / 0.531 0.335–0.719	0.876 0.780–0.954 / 0.382 0.219–0.548	0.953 0.883–0.993 / 0.758 0.597–0.894	0.983 0.964–0.997 / 0.864 0.733–0.967
PSVT	0.787 0.551–1.000 / 0.346 0.002–1.000	0.999 0.997–1.000 / 0.701 0.222–1.000	0.998 0.994–1.000 / 0.451 0.133–1.000	1.000 0.998–1.000 / 0.790 0.333–1.000
SARRH	0.622 0.554–0.692 / 0.068 0.049–0.095	0.616 0.551–0.678 / 0.062 0.046–0.087	0.681 0.625–0.740 / 0.088 0.061–0.126	0.957 0.942–0.970 / 0.524 0.421–0.621
SBRAD	0.827 0.770–0.876 / 0.204 0.131–0.304	0.901 0.856–0.936 / 0.388 0.275–0.516	0.958 0.940–0.973 / 0.508 0.396–0.624	0.956 0.935–0.973 / 0.583 0.468–0.691
SR	0.689 0.660–0.721 / 0.870 0.853–0.887	0.782 0.755–0.809 / 0.916 0.903–0.930	0.887 0.867–0.905 / 0.961 0.952–0.969	0.955 0.943–0.964 / 0.987 0.984–0.990
STACH	0.891 0.863–0.918 / 0.262 0.198–0.342	0.975 0.967–0.982 / 0.530 0.440–0.637	0.988 0.984–0.993 / 0.750 0.651–0.842	0.991 0.978–0.999 / 0.914 0.834–0.973
SVARR	0.873 0.794–0.939 / 0.056 0.026–0.105	0.654 0.550–0.748 / 0.011 0.008–0.015	0.937 0.882–0.977 / 0.382 0.150–0.623	0.886 0.797–0.963 / 0.304 0.114–0.565
SVTAC	0.781 0.574–0.998 / 0.117 0.003–0.447	0.982 0.971–0.989 / 0.060 0.037–0.107	0.988 0.973–1.000 / 0.297 0.043–0.750	0.998 0.996–1.000 / 0.429 0.214–0.833
TRIGU	0.336 0.144–0.530 / 0.001 0.001–0.002	0.602 0.354–0.843 / 0.003 0.001–0.006	0.596 0.193–0.986 / 0.020 0.001–0.062	0.977 0.965–0.988 / 0.038 0.024–0.074

Table 21. Performance for every task in PTB-XL FORM. Each cell reports AUROC (top line) and AUPRC (bottom line) with 95% confidence intervals.

Task	Random	CLOCS	MERL	D-BETA
ABQRS	0.676 0.641–0.713 / 0.529 0.483–0.579	0.691 0.655–0.724 / 0.526 0.480–0.572	0.785 0.753–0.815 / 0.683 0.636–0.727	0.785 0.754–0.814 / 0.649 0.601–0.696
DIG	0.588 0.495–0.677 / 0.027 0.021–0.037	0.664 0.520–0.781 / 0.063 0.028–0.144	0.863 0.793–0.921 / 0.132 0.069–0.233	0.886 0.817–0.944 / 0.214 0.094–0.381
HVOLT	0.838 0.758–0.907 / 0.030 0.018–0.049	0.863 0.756–0.948 / 0.065 0.020–0.191	0.948 0.910–0.976 / 0.095 0.052–0.159	0.900 0.837–0.951 / 0.053 0.028–0.095
INVT	0.753 0.672–0.824 / 0.088 0.058–0.136	0.868 0.824–0.906 / 0.144 0.101–0.212	0.914 0.872–0.947 / 0.293 0.175–0.431	0.903 0.855–0.945 / 0.337 0.201–0.488
LNGQT	0.532 0.356–0.680 / 0.016 0.011–0.024	0.724 0.566–0.847 / 0.043 0.021–0.094	0.819 0.655–0.976 / 0.243 0.073–0.483	0.871 0.803–0.936 / 0.193 0.043–0.424
LOWT	0.632 0.562–0.698 / 0.070 0.057–0.088	0.738 0.674–0.801 / 0.129 0.088–0.191	0.808 0.745–0.862 / 0.213 0.129–0.315	0.837 0.781–0.880 / 0.186 0.133–0.269
LPR	0.692 0.612–0.764 / 0.098 0.058–0.158	0.581 0.476–0.678 / 0.058 0.041–0.084	0.950 0.929–0.969 / 0.490 0.360–0.646	0.961 0.941–0.977 / 0.467 0.341–0.625
LVOLT	0.787 0.706–0.863 / 0.083 0.043–0.179	0.894 0.843–0.937 / 0.191 0.088–0.339	0.898 0.855–0.939 / 0.205 0.094–0.366	0.774 0.680–0.855 / 0.121 0.040–0.273
NDT	0.687 0.640–0.726 / 0.375 0.319–0.436	0.794 0.757–0.825 / 0.453 0.394–0.510	0.866 0.833–0.893 / 0.634 0.563–0.705	0.864 0.835–0.890 / 0.602 0.532–0.672
NST_	0.637 0.576–0.698 / 0.147 0.112–0.194	0.659 0.588–0.727 / 0.224 0.152–0.315	0.772 0.721–0.821 / 0.263 0.196–0.346	0.754 0.695–0.811 / 0.285 0.206–0.375
NT_	0.634 0.551–0.714 / 0.085 0.059–0.125	0.672 0.598–0.742 / 0.092 0.065–0.129	0.817 0.762–0.864 / 0.175 0.115–0.265	0.804 0.744–0.858 / 0.178 0.117–0.256
PAC	0.659 0.585–0.730 / 0.084 0.058–0.127	0.628 0.545–0.709 / 0.087 0.057–0.138	0.676 0.596–0.751 / 0.108 0.064–0.186	0.983 0.973–0.991 / 0.680 0.546–0.837
PRC(S)	0.838 0.813–0.866 / 0.007 0.006–0.008	0.725 0.696–0.753 / 0.004 0.004–0.005	0.829 0.803–0.856 / 0.007 0.006–0.008	0.991 0.984–0.997 / 0.125 0.067–0.250
PVC	0.797 0.749–0.840 / 0.432 0.348–0.518	0.777 0.730–0.824 / 0.338 0.278–0.419	0.870 0.838–0.901 / 0.522 0.439–0.616	0.994 0.991–0.997 / 0.960 0.932–0.982
QWAVE	0.582 0.510–0.659 / 0.090 0.067–0.127	0.558 0.475–0.641 / 0.106 0.069–0.167	0.663 0.599–0.727 / 0.105 0.080–0.139	0.751 0.691–0.809 / 0.182 0.124–0.260
STD_	0.677 0.622–0.723 / 0.194 0.157–0.236	0.682 0.626–0.736 / 0.233 0.182–0.293	0.755 0.704–0.800 / 0.338 0.260–0.422	0.750 0.700–0.795 / 0.289 0.224–0.361
STE_	0.561 0.338–0.712 / 0.006 0.004–0.011	0.574 0.127–0.876 / 0.010 0.004–0.027	0.928 0.841–0.990 / 0.091 0.020–0.273	0.520 0.257–0.930 / 0.013 0.004–0.047
TAB_	0.604 0.382–0.850 / 0.008 0.004–0.022	0.704 0.640–0.762 / 0.009 0.007–0.013	0.868 0.792–0.970 / 0.035 0.013–0.107	0.657 0.493–0.908 / 0.011 0.005–0.036
VCLVH	0.717 0.664–0.766 / 0.199 0.156–0.258	0.820 0.773–0.865 / 0.312 0.250–0.391	0.833 0.790–0.869 / 0.346 0.270–0.432	0.759 0.701–0.809 / 0.276 0.209–0.354

D.2. PTB-XL Results When Labels with Minimal Examples Are Removed

Table 22. ORIG uses the standard PTB-XL SUB test set; CLEAN excludes labels with fewer than 10 positive test examples. Values are macro-AUROC with 95% confidence intervals.

Method	ORIG	CLEAN	ΔMacro-AUROC
RANDOM	0.838 0.813–0.863	0.851 0.838–0.864	+0.013
CLOCS	0.782 0.754–0.811	0.804 0.787–0.820	+0.022
MERL	0.903 0.887–0.916	0.900 0.887–0.911	-0.003
D-BETA	0.893 0.880–0.906	0.896 0.885–0.905	+0.002

Table 23. ORIG uses the standard PTB-XL RHYTHM test set; CLEAN excludes labels with fewer than 10 positive test examples. Values are macro-AUROC with 95% confidence intervals.

Method	ORIG	CLEAN	ΔMacro-AUROC
RANDOM	0.746 0.698–0.791	0.801 0.777–0.823	+0.054
CLOCS	0.825 0.790–0.857	0.805 0.783–0.827	-0.020
MERL	0.886 0.839–0.933	0.912 0.897–0.925	+0.026
D-BETA	0.969 0.957–0.978	0.958 0.942–0.971	-0.011

Table 24. ORIG uses the standard PTB-XL FORM test set; CLEAN excludes labels with fewer than 10 positive test examples. Values are macro-AUROC with 95% confidence intervals.

Method	ORIG	CLEAN	ΔMacro-AUROC
RANDOM	0.678 0.656–0.699	0.754 0.734–0.774	+0.076
CLOCS	0.717 0.690–0.741	0.716 0.694–0.736	-0.001
MERL	0.835 0.820–0.851	0.819 0.802–0.834	-0.016
D-BETA	0.829 0.806–0.853	0.846 0.831–0.858	+0.017

E. Complete Evaluation on CPSC2018

Table 25. Performance on CPSC2018 sub-tasks. Each cell reports AUROC (top line) and AUPRC (bottom line), each with a 95% confidence interval.

Task	Random	CLOCS	MERL	D-BETA
AF	0.882 0.856–0.908 / 0.671 0.613–0.732	0.811 0.780–0.840 / 0.506 0.447–0.562	0.984 0.976–0.991 / 0.935 0.902–0.962	0.995 0.991–0.997 / 0.979 0.967–0.988
IAVB	0.795 0.754–0.831 / 0.312 0.261–0.373	0.760 0.719–0.795 / 0.254 0.212–0.305	0.979 0.965–0.988 / 0.904 0.868–0.937	0.986 0.973–0.996 / 0.952 0.924–0.974
LBBB	0.981 0.948–0.999 / 0.902 0.812–0.975	0.975 0.944–0.994 / 0.817 0.711–0.907	0.990 0.971–1.000 / 0.948 0.892–0.990	0.990 0.970–1.000 / 0.956 0.903–0.995
NSR	0.882 0.862–0.902 / 0.511 0.452–0.576	0.868 0.845–0.891 / 0.512 0.448–0.576	0.936 0.921–0.951 / 0.730 0.678–0.782	0.963 0.953–0.972 / 0.798 0.749–0.845
PAC	0.683 0.631–0.733 / 0.170 0.136–0.215	0.563 0.509–0.617 / 0.111 0.090–0.142	0.807 0.772–0.846 / 0.281 0.225–0.351	0.906 0.870–0.934 / 0.663 0.577–0.738
PVC	0.722 0.667–0.773 / 0.395 0.319–0.476	0.720 0.681–0.758 / 0.218 0.182–0.264	0.818 0.779–0.854 / 0.452 0.376–0.535	0.930 0.904–0.953 / 0.802 0.743–0.854
RBBB	0.953 0.941–0.965 / 0.897 0.868–0.924	0.939 0.925–0.954 / 0.852 0.816–0.888	0.986 0.980–0.990 / 0.959 0.941–0.975	0.980 0.972–0.987 / 0.951 0.933–0.968
STD	0.872 0.843–0.898 / 0.492 0.430–0.565	0.813 0.780–0.846 / 0.424 0.357–0.495	0.955 0.937–0.971 / 0.817 0.769–0.864	0.956 0.942–0.969 / 0.792 0.736–0.850
STE	0.873 0.812–0.927 / 0.309 0.209–0.436	0.830 0.768–0.886 / 0.307 0.194–0.430	0.927 0.887–0.962 / 0.514 0.388–0.645	0.904 0.834–0.959 / 0.559 0.432–0.687

F. Complete Evaluation on CSN

Table 26. Performance on CSN sub-tasks whose labels begin with letter A through M. Each cell reports AUROC (top line) and AUPRC (bottom line), each with a 95% confidence interval.

Task	Random	CLOCS	MERL	D-BETA
1AVB	0.741 0.700–0.782 / 0.069 0.052–0.090	0.685 0.642–0.727 / 0.050 0.038–0.070	0.983 0.977–0.988 / 0.627 0.553–0.703	0.988 0.982–0.992 / 0.754 0.689–0.812
2AVB	0.484 0.100–0.797 / 0.001 0.001–0.003	0.973 0.939–0.994 / 0.036 0.011–0.089	0.990 0.982–0.995 / 0.052 0.027–0.097	0.993 0.987–0.998 / 0.126 0.035–0.387
2AVB1	0.412 0.264–0.601 / 0.001 0.001–0.001	0.591 0.122–0.924 / 0.002 0.001–0.006	0.908 0.816–0.964 / 0.006 0.003–0.013	0.993 0.986–1.000 / 0.205 0.027–0.686
AF	0.877 0.863–0.890 / 0.444 0.412–0.480	0.832 0.816–0.847 / 0.342 0.315–0.370	0.973 0.968–0.976 / 0.748 0.718–0.779	0.975 0.972–0.979 / 0.753 0.717–0.788
AFIB	0.870 0.852–0.885 / 0.194 0.171–0.218	0.835 0.813–0.856 / 0.200 0.172–0.233	0.955 0.949–0.960 / 0.385 0.342–0.433	0.967 0.962–0.971 / 0.545 0.492–0.598
ALS	0.974 0.967–0.981 / 0.490 0.432–0.557	0.845 0.819–0.870 / 0.173 0.138–0.215	0.948 0.932–0.960 / 0.400 0.338–0.464	0.984 0.977–0.990 / 0.683 0.620–0.750
APB	0.658 0.612–0.703 / 0.048 0.038–0.062	0.672 0.633–0.713 / 0.044 0.035–0.057	0.801 0.766–0.835 / 0.095 0.076–0.120	0.981 0.968–0.991 / 0.752 0.690–0.810
AQW	0.878 0.842–0.912 / 0.183 0.144–0.238	0.777 0.725–0.826 / 0.179 0.116–0.246	0.934 0.906–0.959 / 0.379 0.298–0.467	0.969 0.955–0.981 / 0.539 0.455–0.626
ARS	0.961 0.936–0.979 / 0.416 0.341–0.502	0.883 0.853–0.910 / 0.128 0.098–0.166	0.925 0.902–0.944 / 0.250 0.187–0.322	0.902 0.876–0.925 / 0.241 0.168–0.318
AT	0.687 0.589–0.776 / 0.032 0.017–0.053	0.798 0.736–0.849 / 0.030 0.020–0.042	0.885 0.832–0.930 / 0.091 0.053–0.142	0.973 0.963–0.982 / 0.293 0.192–0.417
AVB	0.842 0.762–0.907 / 0.063 0.038–0.108	0.846 0.790–0.894 / 0.060 0.031–0.108	0.928 0.898–0.953 / 0.114 0.069–0.183	0.958 0.943–0.971 / 0.134 0.088–0.204
AVRT	0.519 0.009–0.995 / 0.020 0.000–0.094	0.758 0.382–0.998 / 0.048 0.001–0.200	0.749 0.540–0.993 / 0.013 0.001–0.060	0.851 0.609–0.988 / 0.012 0.001–0.039
CCR	0.893 0.816–0.945 / 0.062 0.028–0.132	0.821 0.736–0.894 / 0.068 0.023–0.157	0.923 0.887–0.954 / 0.097 0.042–0.191	0.848 0.794–0.903 / 0.035 0.016–0.074
CR	0.896 0.798–0.970 / 0.122 0.050–0.240	0.896 0.787–0.981 / 0.138 0.055–0.276	0.935 0.863–0.985 / 0.142 0.054–0.281	0.930 0.858–0.978 / 0.064 0.032–0.127
ERV	0.942 0.906–0.968 / 0.189 0.125–0.268	0.928 0.900–0.951 / 0.163 0.093–0.257	0.962 0.937–0.980 / 0.286 0.186–0.397	0.966 0.953–0.977 / 0.200 0.137–0.288
FQRS	0.958 0.953–0.963 / 0.004 0.003–0.004	0.942 0.936–0.947 / 0.003 0.002–0.003	0.993 0.991–0.995 / 0.022 0.017–0.030	0.995 0.994–0.997 / 0.032 0.024–0.045
IVB	0.772 0.717–0.824 / 0.078 0.050–0.114	0.797 0.758–0.838 / 0.071 0.047–0.102	0.878 0.849–0.904 / 0.094 0.070–0.125	0.968 0.952–0.981 / 0.453 0.364–0.552
JEB	0.633 0.385–0.884 / 0.005 0.001–0.022	0.720 0.518–0.925 / 0.004 0.001–0.015	0.728 0.439–0.976 / 0.008 0.001–0.020	0.966 0.935–0.996 / 0.042 0.007–0.115
JPT	0.115 0.107–0.123 / 0.000 0.000–0.000	0.034 0.030–0.039 / 0.000 0.000–0.000	0.847 0.838–0.855 / 0.001 0.001–0.001	0.783 0.773–0.793 / 0.001 0.001–0.001
LFBBB	0.974 0.940–0.997 / 0.576 0.443–0.730	0.928 0.872–0.969 / 0.373 0.225–0.531	0.989 0.982–0.994 / 0.583 0.438–0.719	0.995 0.992–0.998 / 0.721 0.588–0.841
LVH	0.909 0.804–0.987 / 0.208 0.110–0.346	0.987 0.979–0.993 / 0.287 0.180–0.428	0.943 0.870–0.991 / 0.368 0.216–0.550	0.951 0.899–0.984 / 0.144 0.085–0.221
LVQRSAL	0.888 0.857–0.916 / 0.183 0.143–0.226	0.873 0.842–0.902 / 0.190 0.144–0.248	0.931 0.910–0.948 / 0.288 0.224–0.358	0.805 0.768–0.841 / 0.139 0.095–0.189
MISW	0.791 0.560–0.965 / 0.058 0.004–0.181	0.877 0.740–0.971 / 0.052 0.004–0.170	0.963 0.916–0.994 / 0.101 0.016–0.261	0.915 0.791–0.994 / 0.181 0.015–0.509

Table 27. Performance on CSN sub-tasks whose labels begin with letter P through Z. Each cell reports AUROC (top line) and AUPRC (bottom line), each with a 95% confidence interval.

Task	Random	CLOCS	MERL	D-BETA
PRIE	0.463 0.206–0.716 / 0.001 0.001–0.002	0.654 0.426–0.839 / 0.002 0.001–0.003	0.912 0.808–0.988 / 0.022 0.005–0.054	0.851 0.648–0.982 / 0.153 0.003–0.602
PWC	0.806 0.688–0.907 / 0.025 0.011–0.048	0.717 0.553–0.855 / 0.038 0.008–0.105	0.855 0.743–0.954 / 0.120 0.038–0.259	0.825 0.725–0.907 / 0.050 0.012–0.131
QTIE	0.706 0.596–0.800 / 0.018 0.009–0.034	0.742 0.669–0.811 / 0.030 0.012–0.063	0.931 0.891–0.965 / 0.200 0.090–0.356	0.926 0.873–0.966 / 0.248 0.117–0.400
RAH	0.951 0.946–0.956 / 0.003 0.003–0.004	0.813 0.803–0.823 / 0.001 0.001–0.001	0.999 0.999–1.000 / 0.255 0.111–0.500	0.997 0.995–0.998 / 0.050 0.032–0.083
RBBB	0.976 0.952–0.993 / 0.686 0.592–0.791	0.948 0.918–0.971 / 0.441 0.359–0.537	0.997 0.995–0.998 / 0.885 0.831–0.931	0.997 0.994–0.999 / 0.929 0.883–0.963
RVH	0.862 0.625–0.994 / 0.102 0.013–0.324	0.904 0.787–0.986 / 0.059 0.008–0.174	0.969 0.944–0.990 / 0.092 0.019–0.253	0.994 0.989–0.999 / 0.407 0.102–0.731
SA	0.752 0.728–0.779 / 0.248 0.213–0.283	0.749 0.729–0.770 / 0.189 0.164–0.217	0.835 0.813–0.852 / 0.424 0.378–0.471	0.985 0.983–0.988 / 0.838 0.807–0.867
SB	0.932 0.927–0.937 / 0.885 0.874–0.896	0.975 0.971–0.978 / 0.949 0.940–0.957	0.994 0.992–0.995 / 0.987 0.981–0.991	0.999 0.999–1.000 / 0.999 0.998–1.000
SR	0.741 0.727–0.755 / 0.396 0.375–0.417	0.891 0.882–0.900 / 0.708 0.683–0.730	0.958 0.952–0.963 / 0.873 0.858–0.889	0.993 0.990–0.995 / 0.980 0.976–0.985
ST	0.935 0.926–0.942 / 0.689 0.661–0.719	0.964 0.959–0.968 / 0.802 0.778–0.827	0.991 0.989–0.994 / 0.955 0.941–0.968	0.997 0.995–0.999 / 0.987 0.982–0.992
STDD	0.884 0.841–0.920 / 0.165 0.121–0.218	0.871 0.829–0.908 / 0.179 0.126–0.248	0.962 0.946–0.975 / 0.386 0.303–0.479	0.958 0.944–0.971 / 0.368 0.281–0.459
STE	0.883 0.844–0.917 / 0.117 0.082–0.163	0.773 0.707–0.832 / 0.091 0.055–0.147	0.929 0.896–0.958 / 0.328 0.233–0.427	0.912 0.881–0.940 / 0.282 0.193–0.380
STTC	0.878 0.855–0.900 / 0.201 0.162–0.245	0.846 0.818–0.871 / 0.167 0.131–0.213	0.937 0.923–0.949 / 0.327 0.273–0.385	0.927 0.912–0.941 / 0.275 0.231–0.327
STTU	0.772 0.689–0.856 / 0.033 0.016–0.063	0.702 0.588–0.805 / 0.061 0.021–0.130	0.904 0.853–0.945 / 0.161 0.066–0.298	0.883 0.823–0.931 / 0.156 0.058–0.283
SVT	0.955 0.928–0.976 / 0.540 0.446–0.634	0.980 0.963–0.989 / 0.554 0.472–0.637	0.995 0.992–0.997 / 0.811 0.735–0.882	0.997 0.995–0.998 / 0.886 0.839–0.926
TWC	0.865 0.852–0.878 / 0.515 0.487–0.545	0.840 0.827–0.854 / 0.484 0.453–0.515	0.925 0.916–0.933 / 0.700 0.672–0.727	0.900 0.888–0.911 / 0.664 0.632–0.695
TWO	0.903 0.883–0.921 / 0.249 0.208–0.294	0.868 0.842–0.893 / 0.221 0.182–0.265	0.941 0.926–0.956 / 0.431 0.371–0.494	0.951 0.941–0.960 / 0.392 0.335–0.454
UW	0.856 0.760–0.938 / 0.015 0.006–0.031	0.905 0.870–0.941 / 0.015 0.008–0.038	0.961 0.932–0.985 / 0.155 0.032–0.357	0.941 0.895–0.981 / 0.054 0.016–0.135
VB	0.696 0.685–0.707 / 0.001 0.000–0.001	0.479 0.466–0.490 / 0.000 0.000–0.000	0.653 0.641–0.664 / 0.000 0.000–0.000	0.995 0.994–0.997 / 0.034 0.024–0.050
VEB	0.512 0.267–0.764 / 0.044 0.001–0.216	0.596 0.340–0.820 / 0.003 0.001–0.007	0.856 0.710–0.978 / 0.031 0.006–0.078	0.965 0.929–0.994 / 0.071 0.019–0.183
VET	0.682 0.450–0.888 / 0.001 0.001–0.003	0.841 0.822–0.858 / 0.002 0.001–0.002	0.587 0.337–0.813 / 0.001 0.000–0.002	0.996 0.993–0.999 / 0.079 0.041–0.182
VFW	0.488 0.202–0.771 / 0.210 0.001–0.601	0.507 0.203–0.808 / 0.002 0.001–0.005	0.759 0.434–0.951 / 0.006 0.002–0.015	0.938 0.835–0.995 / 0.223 0.008–0.618
VPB	0.887 0.826–0.939 / 0.088 0.055–0.131	0.831 0.766–0.888 / 0.037 0.026–0.052	0.920 0.885–0.949 / 0.098 0.055–0.161	0.991 0.986–0.995 / 0.506 0.368–0.649
VPE	0.374 0.028–0.983 / 0.006 0.000–0.028	0.981 0.952–1.000 / 0.253 0.010–0.750	0.849 0.555–0.999 / 0.119 0.001–0.333	0.987 0.962–1.000 / 0.339 0.012–0.833
WPW	0.989 0.980–0.997 / 0.250 0.072–0.530	0.955 0.908–0.990 / 0.164 0.016–0.418	0.997 0.995–0.999 / 0.345 0.145–0.604	0.973 0.950–0.992 / 0.317 0.033–0.643

G. Complete Evaluation on EchoNext

Table 28. Performance on EchoNext sub-tasks. Each cell reports AUROC (top line) and AUPRC (bottom line), each with a 95% confidence interval.

Task	Random	CLOCS	MERL	D-BETA
AR	0.684 0.609–0.752 / 0.035 0.023–0.055	0.610 0.535–0.685 / 0.040 0.017–0.086	0.757 0.701–0.807 / 0.045 0.027–0.078	0.640 0.580–0.700 / 0.020 0.015–0.027
AS	0.761 0.731–0.790 / 0.189 0.156–0.227	0.696 0.662–0.728 / 0.138 0.113–0.169	0.799 0.771–0.826 / 0.220 0.180–0.258	0.767 0.739–0.792 / 0.144 0.124–0.170
LVEF ≤ 45	0.859 0.845–0.873 / 0.616 0.583–0.646	0.778 0.760–0.796 / 0.483 0.450–0.515	0.876 0.862–0.888 / 0.646 0.615–0.677	0.861 0.848–0.874 / 0.606 0.576–0.636
LVWT ≥ 13	0.743 0.727–0.760 / 0.416 0.391–0.443	0.670 0.651–0.688 / 0.341 0.319–0.364	0.740 0.725–0.757 / 0.412 0.387–0.438	0.718 0.702–0.734 / 0.353 0.331–0.375
MR	0.792 0.766–0.818 / 0.239 0.202–0.278	0.723 0.693–0.751 / 0.169 0.144–0.200	0.802 0.777–0.826 / 0.234 0.202–0.269	0.793 0.767–0.817 / 0.218 0.186–0.253
PASP ≥ 45	0.744 0.724–0.762 / 0.309 0.282–0.338	0.697 0.677–0.718 / 0.241 0.221–0.263	0.751 0.731–0.770 / 0.324 0.295–0.357	0.731 0.711–0.751 / 0.294 0.265–0.322
PEFF	0.717 0.657–0.772 / 0.031 0.022–0.045	0.631 0.568–0.696 / 0.023 0.017–0.033	0.727 0.669–0.785 / 0.038 0.025–0.063	0.692 0.629–0.756 / 0.031 0.022–0.043
PR	0.770 0.650–0.871 / 0.028 0.009–0.069	0.830 0.779–0.876 / 0.013 0.009–0.019	0.868 0.812–0.920 / 0.057 0.018–0.128	0.825 0.749–0.886 / 0.029 0.011–0.070
RVSD	0.843 0.822–0.863 / 0.351 0.313–0.389	0.793 0.770–0.814 / 0.274 0.241–0.312	0.854 0.834–0.873 / 0.413 0.368–0.463	0.851 0.833–0.868 / 0.368 0.328–0.411
SHD	0.805 0.793–0.817 / 0.772 0.757–0.787	0.722 0.708–0.736 / 0.686 0.669–0.702	0.809 0.798–0.820 / 0.779 0.763–0.792	0.801 0.789–0.812 / 0.762 0.747–0.778
TR-MAX ≥ 32	0.736 0.707–0.762 / 0.197 0.168–0.230	0.691 0.667–0.714 / 0.127 0.113–0.144	0.744 0.720–0.768 / 0.189 0.159–0.222	0.711 0.684–0.738 / 0.157 0.137–0.180
TR	0.785 0.760–0.811 / 0.224 0.193–0.258	0.717 0.689–0.743 / 0.142 0.123–0.162	0.812 0.788–0.835 / 0.250 0.216–0.289	0.791 0.765–0.815 / 0.235 0.202–0.275